iScience

CellPress
OPEN ACCESS

Article

Retinal glial remodeling by FGF21 preserves retinal function during photoreceptor degeneration

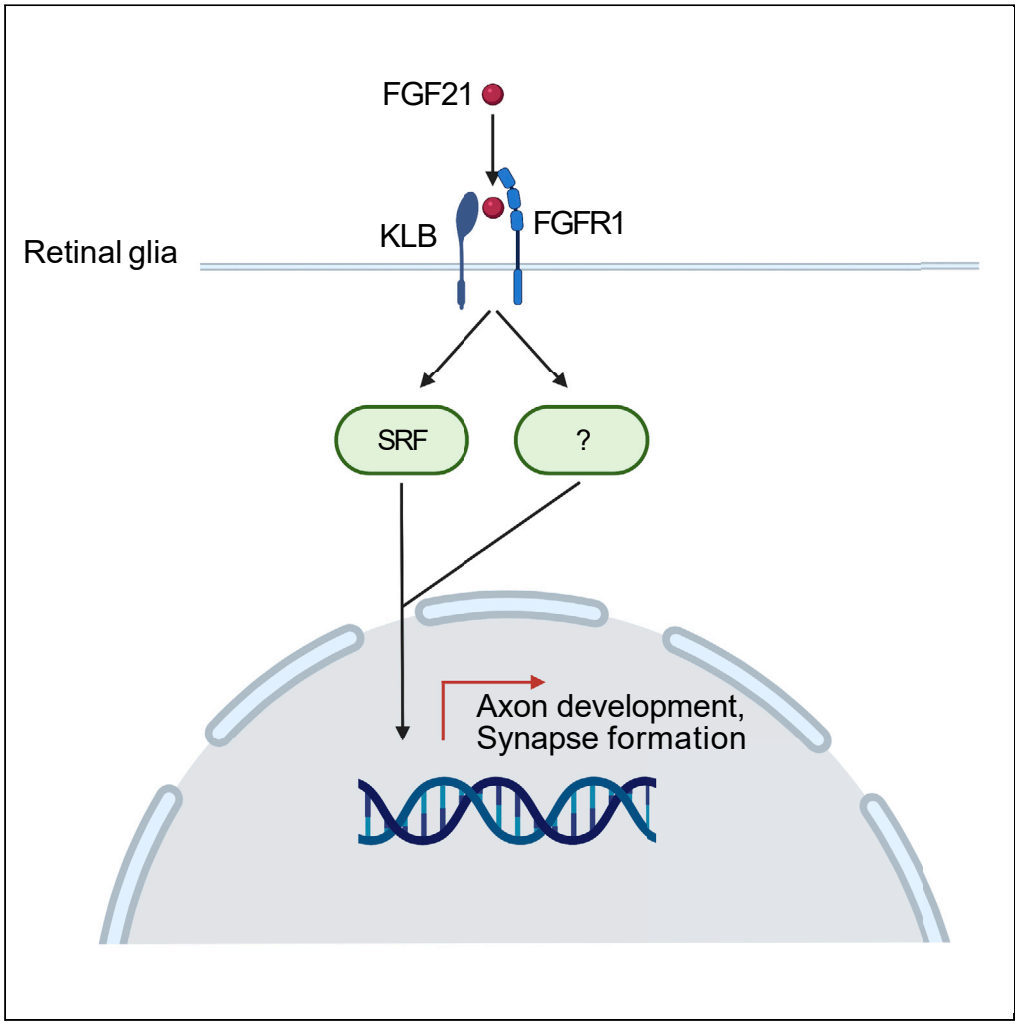

Zhongjie Fu, Chenxi Qiu, Gael Cagnone, ..., Ann Hellström, Saswata Talukdar, Lois E.H. Smith

lois.smith@childrens.harvard.edu

Highlights

FGF21 restores retinal neuronal function and Müller glial cell morphology in mouse RP

Müller glial cells are the primary cells expressing FGF21 receptor in mouse retinas

FGF21 increases Müller glial axon development and synapse formation pathway genes

Synaptic connection between ONL and INL is preserved by FGF21

Fu et al., iScience *24*, 102376
April 23, 2021
https://doi.org/10.1016/j.isci.2021.102376

iScience

CellPress
OPEN ACCESS

Article

Retinal glial remodeling by FGF21 preserves retinal function during photoreceptor degeneration

Zhongjie Fu,[1,2,8] Chenxi Qiu,[3,8] Gael Cagnone,[4,5] Yohei Tomita,[1] Shuo Huang,[1] Bertan Cakir,[1] Yumi Kotoda,[1] William Allen,[1] Edward Bull,[1] James D. Akula,[1] Jean-Sébastien Joyal,[4,5] Ann Hellström,[6] Saswata Talukdar,[7] and Lois E.H. Smith[1,9,*]

SUMMARY

The group of retinal degenerations, retinitis pigmentosa (RP), comprises more than 150 genetic abnormalities affecting photoreceptors. Finding degenerative pathways common to all genetic abnormalities may allow general treatment such as neuroprotection. Neuroprotection may include enhancing the function of cells that directly support photoreceptors, retinal pigment epithelial cells, and Müller glia. Treatment with fibroblast growth factor 21 (FGF21), a neuroprotectant, from postnatal week 4–10, during rod and cone loss in P23H mice (an RP model) with retinal degeneration, preserved photoreceptor function and normalized Müller glial cell morphology. Single-cell transcriptomics of retinal cells showed that FGF21 receptor *Fgfr1* was specifically expressed in Müller glia/astrocytes. Of all retinal cells, FGF21 predominantly affected genes in Müller glia/astrocytes with increased expression of axon development and synapse formation pathway genes. Therefore, enhancing retinal glial axon and synapse formation with neurons may preserve retinal function in RP and may suggest a general therapeutic approach for retinal degenerative diseases.

INTRODUCTION

Retinitis pigmentosa (RP) is a general term for retinal degenerations arising from >150 retinal genetic defects (Newton and Megaw, 2020), affecting about 1 in 4000 people in the USA. RP is typically diagnosed in adolescents and young adults, progressing in most cases to legal blindness by age 40. Most patients with RP have initial loss of rods (with loss of night vision), followed by loss of cones (with loss of color and central vision) as a secondary, "bystander" effect, associated with metabolic dysfunction (Punzo et al., 2009) of cones after loss of rods (Ait-Ali et al., 2015; Punzo et al., 2009). To date, gene therapy has been approved for only one gene defect (RPE65) (Pierce and Bennett, 2015). Therefore, understanding cellular pathways that support photoreceptor function common to all forms of RP may lead to a more generalized therapeutic approach, without having to perform many gene therapy clinical trials for each rare gene defect.

Loss of photoreceptors is followed by significant morphological changes in the inner retinal neurons, known as retinal remodeling (Nagar et al., 2009) which includes dendritic retraction, axonal sprouting, ectopic synapse formation, cell migration, and disruption of stratification (Denlinger et al., 2020; Krishnamoorthy et al., 2016). Following the loss of photoreceptors, both bipolar cells and horizontal cells undergo dendritic retraction (Nagar et al., 2009). Bipolar cells form ectopic synapses with the surviving photoreceptors (Peng et al., 2000) and horizontal cells show axonal growth into the inner nuclear layer and inner plexiform layer (Park et al., 2001). Although amacrine cells and retinal ganglion cells generally maintain their morphology (Krishnamoorthy et al., 2016), some amacrine cells can migrate or sprout processes into the outer plexiform layer (OPL) in response to photoreceptor loss (Park et al., 2004). Retinal ganglion cells also can undergo morphological changes and even migrate to the inner nuclear layer (O'Brien et al., 2014). This remodeling process is accompanied by Müller glial responses (Jones et al., 2016). Müller glia form close contacts with retinal neurons and modulate neuronal activities (Newman and Reichenbach, 1996). In particular, Müller glia are "nurse" cells for photoreceptors as they indirectly connect photoreceptors to blood vessels. Müller glial cells are activated by many stress stimuli and are the first cell class in the

[1]Department of Ophthalmology, Boston Children's Hospital, Harvard Medical School, Boston, MA 02115, USA

[2]The Manton Center for Orphan Disease, Boston Children's Hospital, Harvard Medical School, Boston, MA 02115, USA

[3]Department of Medicine, Division of Translational Therapeutics, Beth Israel Deaconess Medical Center, Harvard Medical School, Boston, MA 02115, USA

[4]Department of Pediatrics, Pharmacology and Ophthalmology, CHU Sainte-Justine Research Center, Université de Montréal, Montreal, Qc H3A 0C4, Canada

[5]Department of Pharmacology and Therapeutics, McGill University, Montreal, Qc H3A 0C4, Canada

[6]Section for Ophthalmology, Department of Clinical Neuroscience, Institute of Neuroscience and Physiology, Sahlgrenska Academy, University of Gothenburg, Göteborg 405 30, Sweden

[7]Cardiometabolic Diseases, Merck Research Laboratories, 33 Avenue Louis Pasteur, Boston, MA 02115, USA

[8]These authors contributed equally

[9]Lead contact

*Correspondence: lois.smith@childrens.harvard.edu

https://doi.org/10.1016/j.isci.2021.102376

neural retina to respond to stress (Bringmann and Wiedemann, 2012). There are several changes in Müller glia during retinal degeneration, including reactive gliosis (Nagar et al., 2009), metabolic alterations (Pfeiffer et al., 2016), expression of mature neuronal proteins (Krishnamoorthy et al., 2016), and phagocytosis of dead photoreceptor cells (Sakami et al., 2019). Müller glial cells also fill the vacated space after the death of photoreceptors, and these new glial surfaces serve as pathways for neuronal migration and process extension (Jones and Marc, 2005). However, there are knowledge gaps regarding the impact of remodeling on retinal function during photoreceptor degeneration.

Photoreceptors do not have direct contact with blood vessels for supply of nutrients, oxygen, recycling of critical molecules, and waste removal. They depend on Müller glial cells and retinal pigment epithelial (RPE) cells (which have contact with both blood vessels and photoreceptors) for these functions which support energy-intensive photoreceptor outer segment renewal, maintenance of the "dark current", and other high energy demand processes (Chen and Anderson, 1993; Fu et al., 2020; Jablonski and Iannaccone, 2000; Mukherjee et al., 2007; Wang et al., 2004). RPE cells have been studied more than Müller glial cells in this capacity. RPE cells support photoreceptors (particularly rods) by transporting glucose from the choriocapillaris to the retina (Ban and Rizzolo, 2000). The RPE cell also directly participates in the visual cycle, including the rate-limiting step of isomerization of the *all-trans retinyl ester* to *11-cis retinol* by RPE65 (Kiser and Palczewski, 2010), and aids outer segment turnover through phagocytosing photoreceptor outer segments shed by rods (Kevany and Palczewski, 2010). Therefore, modulating RPE metabolism may also help improve photoreceptor function during retinal degeneration.

Some neuroprotectants may act by improving the support functions of Müller glia (and/or RPE). We examined the effects of fibroblastic growth factor 21 (FGF21) on the support of Müller glia (and/or RPE) in a model of retinal degeneration (the heterozygous P23H mouse model of RP) as FGF21 has been shown to be neuroprotective in many model systems. FGF21 receptors and co-receptor beta-klotho are expressed in the central nervous system (CNS), and FGF21 has direct effects on the brain (Bookout et al., 2013; Hill et al., 2019; Hultman et al., 2019; Sa-Nguanmoo et al., 2016a). Furthermore, FGF21 increases hippocampal synaptic plasticity (Sa-Nguanmoo et al., 2016b), attenuates cognitive impairment (Wang et al., 2018) in high-fat-diet-induced obese rodents, and protects the brain against d-galactose-induced aging (Yu et al., 2015). FGF21 treatment also improves primary cortical neuronal metabolism by enhancing ketone body utilization *in vitro* (Katsu-Jimenez and Gimenez-Cassina, 2019) and ameliorates neurodegeneration in animal models of Alzheimer disease (Chen et al., 2019). However, studies of the FGF21 pathway in retinal degeneration models of RP are limited, despite the fact that the retina is part of the CNS (London et al., 2013). We previously reported that FGF21 protects against photoreceptor dysfunction and cone outer segment disorganization in type 1 diabetic mice (Fu et al., 2018). In this report, we examined the effect of FGF21 on retinal degeneration in the P23H mouse model of RP.

RESULTS

FGF21 administration protected retinal function in heterozygous P23H mice

Rod and cone Electroretinographies (ERGs) were obtained at postnatal week 4, 7, and 10: scotopic ERGs to assess rod and rod-mediated function and photopic ERGs to assess cone-mediated function. Following the first ERGs, at postnatal week 4, we administered long-acting FGF21 (PF-05231023, 10 mg/kg, twice a week) or vehicle control to littermates intraperitoneally, which was maintained through the final ERG at postnatal week 10 (Figure 1A).

To study rod and rod-mediated retinal function, we presented a series of flashes of doubling intensity, from those that elicited a just detectable b-wave (a measure of mostly bipolar cells) to those that saturated the a-wave (a measure of photoreceptors) (Akula et al., 2010) to the dark-adapted eye. Prior to FGF21 treatment, we recorded ERG responses in P23H mice at postnatal week 4, and all responses at postnatal week 7 and 10 were normalized to postnatal week 4. In P23H mice, amplitudes of both *a*-wave and *b*-wave were attenuated from postnatal week 4–7 (Figure 1B). However, the sensitivity of bipolar cells (*b*-wave) was increased (Figure 1B), suggesting retinal remodeling compensating for rod degeneration (Jones et al., 2016; Krishnamoorthy et al., 2016; Leinonen et al., 2020). In contrast, P23H mice receiving FGF21 had significantly less pronounced rod and bipolar cell amplitude decreases (Figure 1C). FGF21 similarly improved cone function in P23H mice. In vehicle-treated P23H mice, cone b-wave (bipolar cells) amplitude was decreased while sensitivity was increased at postnatal week 10 (Figures 1D and 1E), an effect which was mitigated by FGF21 treatment (Figure 1F). With FGF21 treatment, both female and male P23H mice showed increased

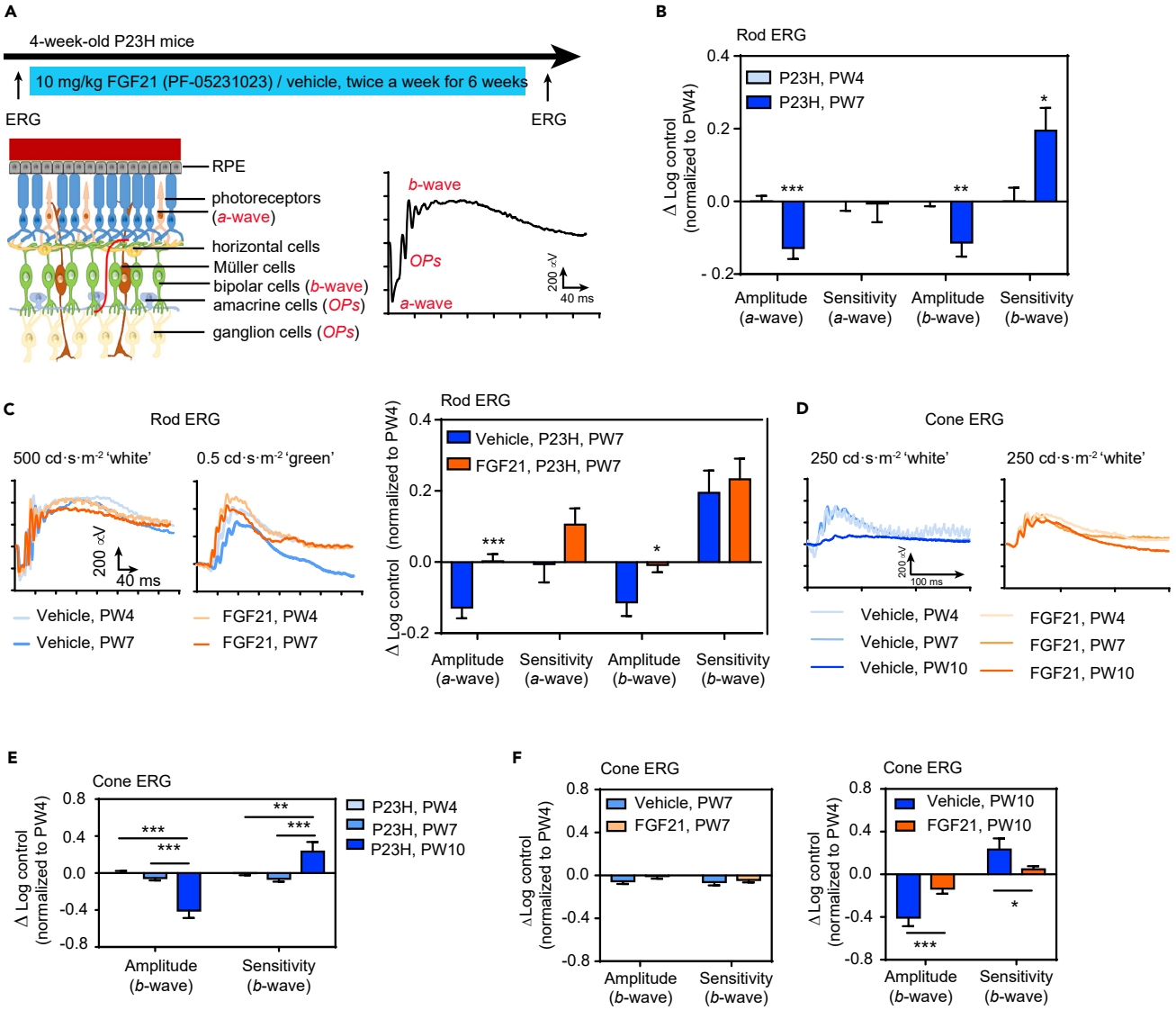

Figure 1. FGF21 administration protects retinal function in P23H mice

ERG plots with "white" (for maximal a-wave) and "green" (for maximal b-wave) light stimulation are shown to demonstrate the parameters: a-wave (photoreceptors), b-wave (bipolar cells), and oscillatory potentials (OPs, amacrine cells, ganglion cells). Neuronal cell amplitude and sensitivity were measured and calculated. All ERG data were presented as the log change from control (ΔLog control) and normalized to that from postnatal week 4 (PW4). Data were presented as mean ± standard error of the mean.

(A) FGF21 (PF-05231023, 10 mg/kg) or vehicle control (PBS) was administered twice a week intraperitoneally to 4-week-old P23H mice. Scotopic (rods) ERG was conducted at postnatal week (PW) 4 and PW7; photopic (cones) ERGs were conducted at PW4, PW7, and PW10.

(B) Overall changes in rod ERG amplitude and sensitivity of rods (*a*-wave) and bipolar cells (*b*-wave) in P23H mice. ERG was conducted at the same mice at PW4 and PW7. Amplitude of rods and bipolar cells was decreased from PW4 to PW7. Sensitivity of bipolar cells was increased as a compensatory response to the decreased amplitude at PW7. n = 24–26 eyes. Multiple t test.

(C) Representative rod ERG plots in P23H mice treated with vehicle or FGF21 at PW4 and PW7. FGF21 treatment attenuates the decrease in amplitude of rods and bipolar cells at PW7. n = 26 eyes (vehicle), n = 26 eyes (PF-05231023). Multiple t test.

(D) Representative cone ERG plots in P23H mice treated with vehicle or PF-05231023 at PW4, PW7, and PW10.

(E) Overall changes in cone ERG amplitude and sensitivity of bipolar cells in P23H mice. ERG was conducted at the same mice at PW4, PW7, and PW10. Amplitude of bipolar cells was decreased from PW7 to PW10. Sensitivity of bipolar cells was increased as a compensatory response to the decreased amplitude at PW10. n = 17–29 eyes. Two-way analysis of variance (ANOVA).

(F) FGF21 treatment attenuates the decrease in amplitude of bipolar cells at PW10 and less induction in sensitivity of bipolar cells in P23H mice. n = 17–30 eyes (vehicle), n = 28–30 eyes (PF-05231023). Multiple t test.

For B-F, *P < 0.05, **P < 0.01, ***P < 0.001.

See also Figures S1 and S2.

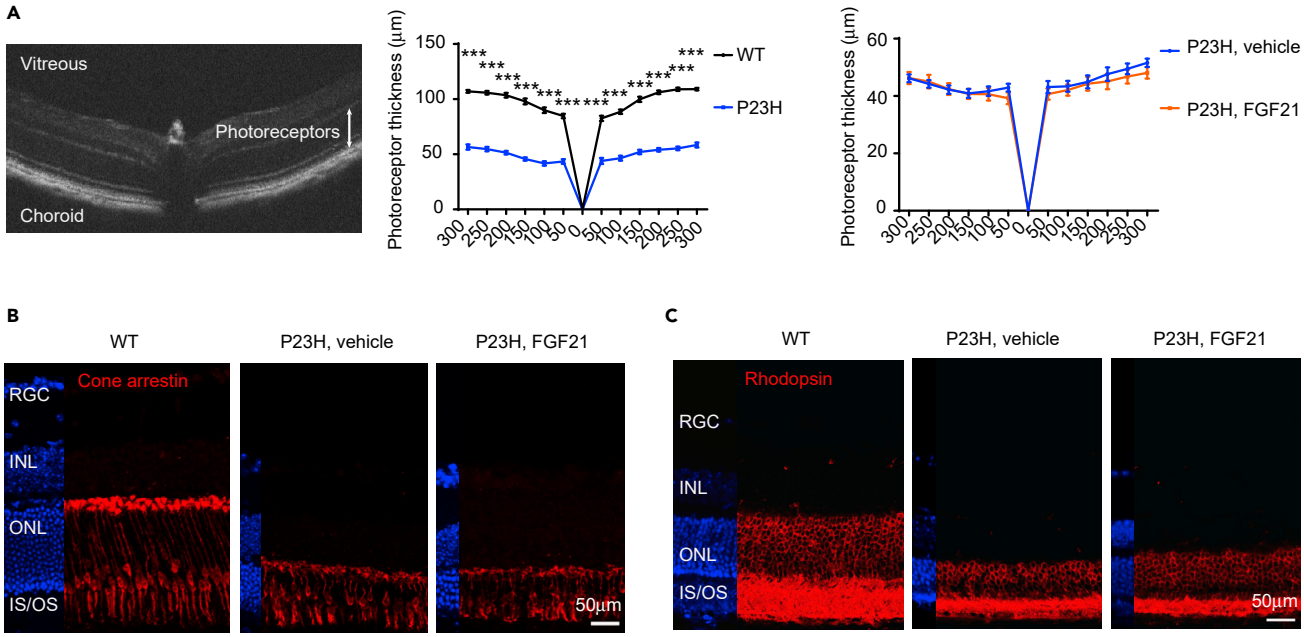

Figure 2. FGF21 administration does not change retinal thickness in P23H mice

(A) Representative OCT images of WT mouse. Photoreceptor thickness (nucleus plus inner/outer segments) was shown as a double-headed arrow. n = 11 eyes (WT), n = 14 eyes (P23H). n = 12 eyes (P23H, vehicle), n = 13 eyes (P23H, FGF21). Multiple t test. ***P < 0.001. Data were presented as mean ± standard error of the mean.

(B and C) FGF21 treatment did not change cone (B) and rod (C) structure in P23H mice at PW10. Cone arrestin (red, for cones) and rhodopsin (red, for rods) signals were shown at ONL and IS/OS layer in WT mice, but the signals were disrupted in both FGF21- and vehicle-treated P23H mice. Littermate mice were used for the three groups. n = 2–4 mice per group. DAPI (blue) was used for nucleus staining. RGCs, retinal ganglion cells; INL, inner nuclear layer, ONL, outer nuclear layer, IS/OS, inner/outer segment. Scale bar, 50 μm.

rod photoreceptor (*a*-wave) amplitude at postnatal week 7, and female mice also had improved rod photoreceptor sensitivity and rod bipolar cell (*b*-wave) amplitude (Figure S1A). FGF21 showed significant protection of the cone pathway in male mice and had a milder impact in female mice at postnatal week 10 (Figure S1B). In addition, we also observed that male vs. female mice showed reduced rod bipolar cell sensitivity during retinal degeneration (Figure S1C), indicating less inner neuronal compensatory effects in males. We further examined the longitudinal impacts of FGF21 on cone pathways from postnatal week 4–13 (Figure S2). We found that cone degeneration was observed as early as postnatal week 7 in this group of P23H mice and FGF21 protected against the loss of cone function until postnatal week 10. However, the protection was no longer observed at postnatal week 13.

FGF21 does not prevent decrease in retinal thickness in P23H mice

We next examined if cone and rod photoreceptor structure was modulated by FGF21 administration. Using optical coherence tomography (OCT), we found ~50% reduction in photoreceptor layer thickness (nuclear layer and inner/outer segment layer) in P23H retinas at postnatal week 10. FGF21 did not influence the loss (Figure 2A). A more refined view of cone and rod photoreceptor structure was examined with immunohistochemistry staining of cone arrestin (for cones) and rhodopsin (for rods). FGF21 did not influence the disruption of rod and cone structures seen in P23H mice (Figures 2B and 2C). Thus, FGF21 improved retinal function in P23H mice despite not preventing gross photoreceptor structural changes.

FGF21 modulates retinal glial responses in P23H mice

To gain insights into protective effects of FGF21 on retinal function and to distinguish a primary effect on photoreceptors from a secondary effect on support cells or other retinal neurons, we used single-cell transcriptomics (profiling ~30,000 cells) to examine cellular and molecular change in different retinal cell types of P23H mouse retinas with FGF21 or vehicle treatment. First, unsupervised t-distributed stochastic neighbor embedding revealed 23 cell clusters with distinct expression profiles, which were subsequently

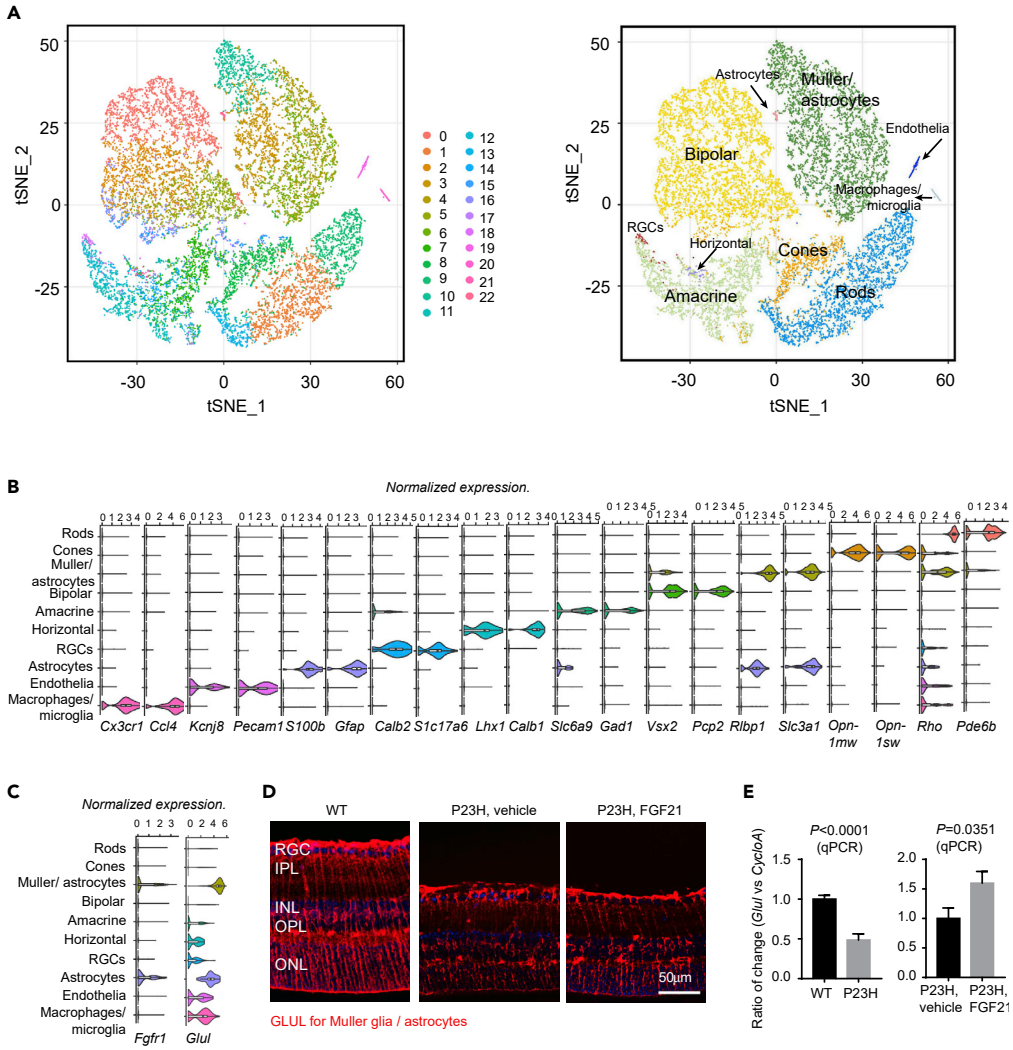

Figure 3. Single-cell transcriptomics of FGF21- vs vehicle-treated P23H littermates at PW10

(A) t-Distributed stochastic neighbor embedding projection of different color-coded retinal cell types from P23H mice treated with PF-05231023 or vehicle controls.

(B) Violin plots of marker gene normalized expression for different cell types. Rho and Pde6b (rods), Opn1mw and Opn1sw (cones), Rlbp1 and Slc3a1 (Müller glia and astrocytes), Vsx2 and Pcp2 (bipolar cells), Slc6a9 and Gad1 (amacrine), Lhx1 and Calb1 (horizontal cells), Calb2 and Slc17a6 (retinal ganglion cells, RGCs), S100b and Gfap (astrocytes), Kcnj8 and Pecam1 (endothelia), Cx3cr1 and Ccl4 (microglia).

(C) Violin plots of FGF21 receptor *Fgfr1* and Müller glial cell and astrocyte marker *Glul* gene normalized expression for different cell types. Fgfr1 was distinctly expressed in Müller glia/astrocyte cell cluster.

(D) FGF21 treatment increased GLUL immunostaining in P23H mice at PW10. GLUL signals were shown across the entire retina in WT mice (n = 3 mice), but the signals were disrupted in vehicle-treated P23H mice (n = 4 mice). GLUL signals were still observed in Müller glial cell processes across the entire retina in FGF21-treated P23H mice (n = 5 mice). DAPI (blue) was used for nucleus staining. Scale bar, 50 μm.

(E) FGF21 treatment increased retinal *Glul* mRNA expression in P23H mice. Retinal *Glul* expression was further examined with qPCR and decreased in P23H versus littermate WT mice at PW10 (n = 3 mice per group). Induced *Glul* expression was observed in FGF21- versus vehicle-treated P23H littermate mice (n = 4 mice per group). Unpaired t test. Data were presented as mean ± standard error of the mean.

See also Figure S3

collapsed into 10 major cell types (Figure 3A). Cell types were identified by correlating expression profiles of individual cells with the published database from the Mouse Cell Atlas and were independently validated by the expression of known markers for each cell type (Figure 3B). We found that putative Müller glial

cell markers (*Rlbp1, Slc1a3*) were also detected in "astrocyte" clusters; hence, it was difficult to precisely distinguish between Müller glia and astrocyte clusters, as we were unable to detect specific genes unique to each cluster. Therefore, we used Müller glia/astrocyte for subsequent analyses.

Interestingly, we found that the FGF21 receptor, *Fgfr1*, was specifically expressed in retinal glia cells (Müller glia/astrocytes) (Figures 3C and S3A), suggesting retinal glia might be a primary target of FGF21 in P23H mouse retinas. Glutamine synthetase (*Glul*) is described in the literature as a cell marker of Müller glia (Haverkamp and Wassle, 2000; Riepe and Norenburg, 1977). Single-cell transcriptomics showed that *Glul* was highly expressed in the Müller glia/astrocyte cluster (Figure 3C) and FGF21 versus vehicle increased *Glul* levels in a Müller glia/astrocyte cluster in P23H mice at postnatal week 10 (logFC = 0.169564, $P < 0.001$). GLUL immunostaining linearly spanned the entire retina in wild-type mice (consistent with the morphology of Müller glia) but showed a disrupted pattern in P23H mice. FGF21 treatment increased GLUL staining in Müller glial cell processes (Figure 3D), suggesting a GLUL increase toward normalization in Müller glia. In P23H retinas, *Glul* mRNA expression was decreased in P23H heterozygous versus littermate wild-type (WT) retinas at postnatal week 10, which was increased with FGF21 treatment (Figure 3E). Our findings suggest that single-cell analysis is a reliable approach for quantitative analysis of gene expression in retinas of P23H mice with FGF21 treatment.

FGF21 facilitates retinal glial remodeling in P23H mice

To assess the transcriptomic impact of FGF21 treatment, we identified differentially expressed genes in the major cell types (rods, cones, Müller glia/astrocytes, bipolar cells, amacrine cells) by comparing FGF21-treated mouse retinas with vehicle-treated littermate controls (Tables S1–S10) using gene ontology analysis. Given the unique expression of *Fgfr1* in the Müller glia/astrocyte cells and the potential primary effects of FGF21 on these cells, we first focused on the genes that are differentially expressed in Müller glia/astrocytes. Gene ontology analysis showed a marked increase in genes involved with axon and synapse development (Figures 4A and 4B), consistent with glia cells controlling the formation of synaptic circuits which was associated with improved neuronal function (Stogsdill and Eroglu, 2017; Vecino et al., 2016). Under physiological conditions, glial fibrillary acidic protein (GFAP) staining by immunohistochemistry is seen only in astrocytes, identified morphologically and by position in retinal cross sections. Only under stressed condition is GFAP induced in Müller glia (Bringmann and Wiedemann, 2012; Eisenfeld et al., 1984). In P23H mice, we found an interrupted linear pattern of GFAP staining of presumed Müller glia as they spanned the retina. With FGF21 treatment of littermate P23H mice, the staining of presumed Müller glia became linear and non-interrupted (Figure 4C), with improved Müller glial cell morphology, in line with more consistent GLUL immunostaining (Figure 3C). FGF21 treatment in wild-type mice did not show changes in GFAP staining (Figure S4). The postsynaptic density protein PSD95 signals are most prominent along the OPL in mammalian retinas (Koulen et al., 1998). The PSD95-positive band along the OPL was thinner in P23H vs. WT mice (Figure 4C). FGF21- vs. vehicle-treated P23H mice showed a thicker PSD95-positive band along the OPL (Figure 4C), suggesting improved synapse connection. Taken together, FGF21 appeared to help normalize Müller glial structure and expression of GLUL and GFAP with increased expression of axon/synapse genes during photoreceptor degeneration.

We also found that FGF21 increased synapse gene pathway expression in amacrine cells (Figure S5A), suggesting that FGF21 also improved other retinal cell connections in P23H mice. ERG responses showed a trend toward increased amplitude and sensitivity of rod oscillatory potentials (OPs) (amacrine cells and ganglion cells) at postnatal week 7 (Figure S5B) and a significant increase in the amplitude of cone OPs at postnatal week 10 (Figure S5C) in FGF21- vs vehicle-treated P23H mice. Taken together, our findings suggest that FGF21 protects retinal function in P23H mice likely through improving cell connections.

FGF21 activates serum response factor in Müller glial cells

To examine the transcriptional program mediating FGF21's effects in promoting axon development and synapse formation, we conducted gene set enrichment analysis to examine other potential common motifs of axon formation associated with the genes affected by FGF21. Notably, serum response factor (SRF) motifs are highly enriched in the FGF21 differentially expressed genes in Müller glia/astrocytes (Figure 5A, NES = 2.4, $P < 0.001$, FDR = 0.001), and *Srf* is specifically expressed in retinal Müller glia/astrocytes and astrocyte clusters (Figure 5B). Single-cell transcriptomics showed that FGF21 versus vehicle increased *Srf* levels in Müller glia/astrocyte cluster in P23H mice at postnatal week 10 (logFC = 0.5515, $P < 0.001$). To further test this association, we treated immortalized rat retinal Müller glia (rMC-1) (Sarthy et al., 1998) *in vitro* with FGF21

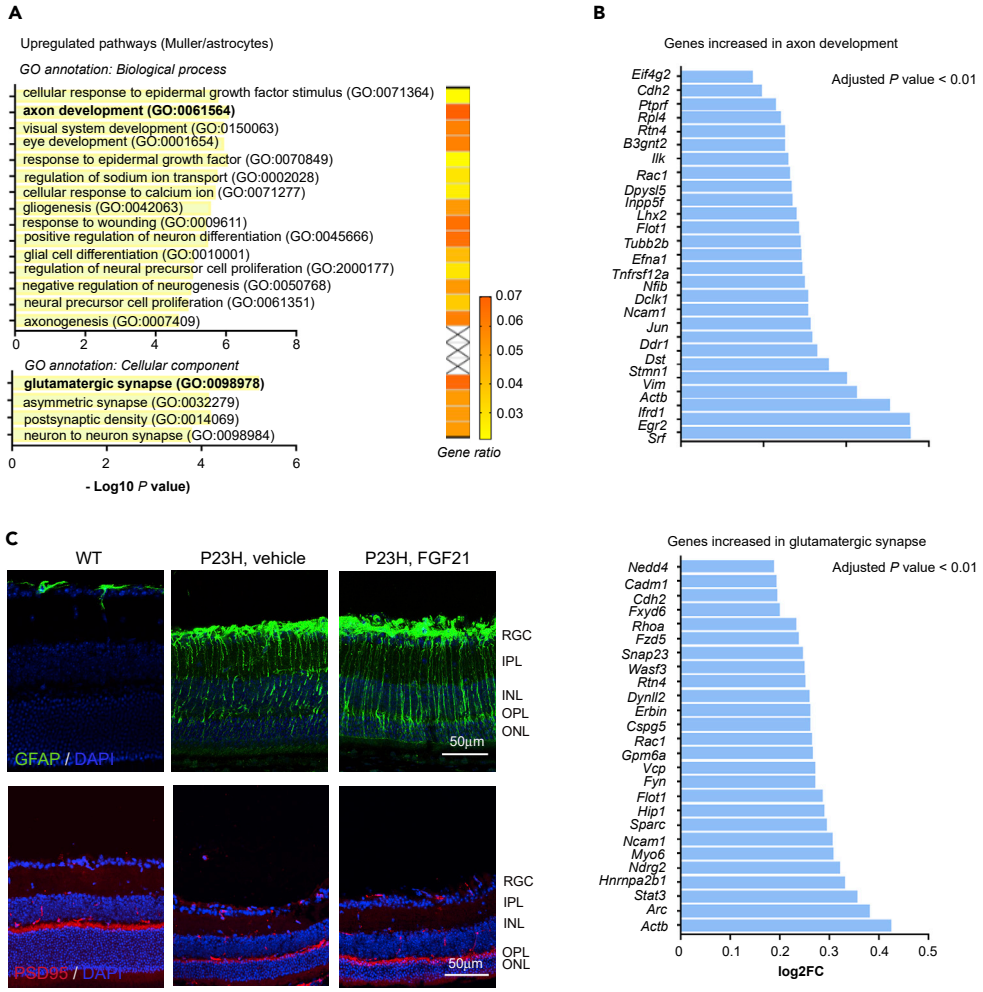

Figure 4. FGF21 activates glial cell remodeling in P23H retinas

(A) Most upregulated genes in Müller glia/astrocyte population by FGF21 are associated with the axonogenesis, neurogenesis, and visual system development-related gene ontology terms. p values for enriched gene ontology (GO) terms are showed in bar graphs ($P < 0.01$). Gene ratio for each pathway was shown in heatmap.

(B) Genes involved in axon development and glutamatergic synapses are upregulated by FGF21 in Müller glia/astrocyte population. Bar graph showing fold change (in log2) of indicated genes in FGF21 vs vehicle control.

(C) FGF21 treatment showed well-structured Müller glia/astrocytes morphology and better synapse connections in P23H mice at PW10. GFAP (green) signals were only shown in astrocytes at RGC layer in WT mice (n = 3 mice). Discrete GFAP signals were induced across the entire retina in vehicle-treated P23H mice (n = 4 mice), but the signals were shown in a better linear structure in FGF21-treated P23H mice (n = 6 mice). PSD95 (red) signals were strong along the OPL in WT mice (n = 3 mice), and the thickness of the PSD95-positive band was thinner along the OPL in vehicle-treated P23H mice (n = 4 mice). FGF21 treatment showed thicker PSD95 band along the OPL in P23H mice (n = 4 mice). DAPI (blue) was used for nucleus staining. RGCs, retinal ganglion cells, IPL, inner plexiform layer, INL, inner nuclear layer, OPL, outer plexiform layer, ONL, outer nuclear layer. Scale bar, 50 μm.

See also Figures S4 and S5.

(50, 250 ng/mL) or vehicle control for 24 hr. FGF21 dose dependently increased SRF protein levels in rMC-1 cells (Figure 5C), consistent with the *in vivo* observation. We speculated that FGF21 via integrin-linked kinase (ILK) increases SRF protein levels. FGF21 vs. vehicle increased *Ilk* (logFC = 0.256994, P = 0.006) in Müller glia/astrocyte cluster. ILK stabilizes SRF protein in human esophageal epithelial cell Het1A *in vitro* (Chai et al., 2007).

FGF21 decreases RPE and rod metabolism in P23H mice

Both RPE and Müller glial cells are in close contact with blood vessels and photoreceptors (Bringmann and Wiedemann, 2012; Pavan and Dalpiaz, 2018). FGF21 receptor *Fgfr1* and its co-receptor beta-klotho were

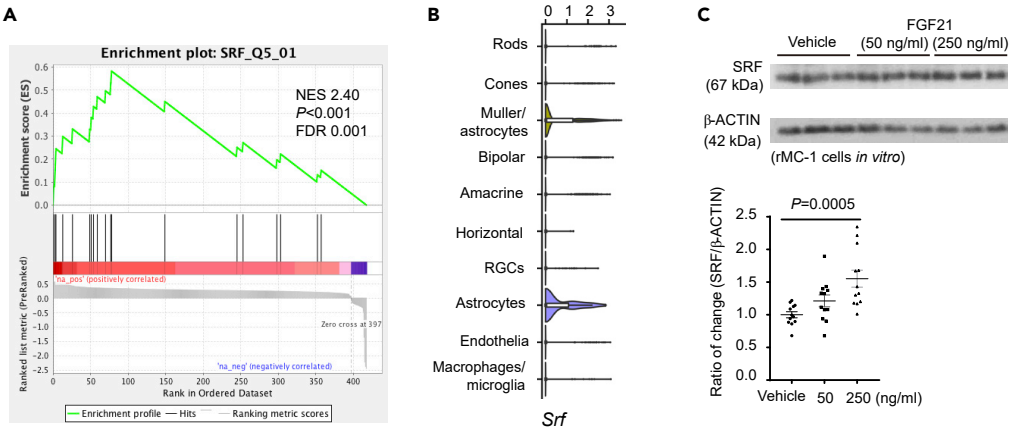

Figure 5. FGF21 activates SRF pathway in retinal glial cells

(A) Gene set enrichment analysis revealed significant enrichment of SRF binding motifs in the differentially expressed genes induced by FGF21 (as compared to the vehicle control).

(B) Violin plots of *Srf* gene normalized expression for different cell types. *Srf* was distinctly expressed in Müller glia/astrocyte and astrocyte cell clusters.

(C) FGF21 treatment upregulated SRF levels in immortalized rat retinal Müller glial cells rMC-1 cells *in vitro*. rMC-1 cells were cultured in DMEM/F12 medium supplemented with 10% FBS and 1% antibiotic/antimycotic. Cells were treated with vehicle (PBS), or 50, 250 ng/mL FGF21 for 24 hr. Western blot analyses for SRF were conducted, and β-ACTIN was used as the internal control. n = 3 for each independent experiment, and the experiments were repeated 4 independent rounds. One-way ANOVA. Data were presented as mean ± standard error of the mean.

also expressed in mouse RPE cells (Figure S3B). To examine if FGF21 also influences RPE cell function, we conducted RNAseq in isolated RPE cells from FGF21- versus vehicle-treated P23H littermates at postnatal week 10. FGF21 treatment significantly decreased expression of genes involved in fatty acid metabolic processes (GO: 0006631, gene ratio = 0.045, $P < 0.001$) in P23H mice (Figures 6A–6C), suggesting that FGF21 modulates RPE cell metabolism, in line with decreased ATP metabolic processes (GO:0046034, gene ratio = 0.054, $P < 0.001$) in rod photoreceptors (Figures 6D and 6E). However, gene ontology analysis also showed that many diverse pathways in RPE cells were affected (Figure S6. Table S11), in contrast to a specific/concerted program observed in Müller glia/astrocytes.

DISCUSSION

We found that administration of FGF21 starting from the onset of rod degeneration in an RP model improved rod and cone ERG function, in association with modulated Müller glial cell responses facilitating axon development and synapse formation.

Retinal modeling of the retinal circuitry in the inner retinal neurons and glial cells occurs concomitant to rod and especially cone dysfunction and loss in RP (Jones et al., 2016; Krishnamoorthy et al., 2016). In phase I, metabolic alterations are first initiated in glial cells in response to photoreceptor stress. There is a high variability in taurine, glutamate, glutamine, glutathione, glutamine synthetase, and cytosolic retinaldehyde-binding protein immunostaining in neighboring Müller cells during degeneration in RP rabbit retinas, while Müller cells in healthy retinas have a very homogeneous metabolic signature (Pfeiffer et al., 2016). In phase II, Müller glia become hypertrophic and retinal glial remodeling follows the progressive loss of photoreceptors. Finally, there is a neural, glial, and vascular remodeling with rewiring through evolution of complex neurite fascicles, new synaptic foci in the inner nuclear layer, and new connections throughout the retina (Jones et al., 2003). Retinal remodeling has been described as a process that can exacerbate retinal degeneration. However, homeostatic plasticity studies in the CNS suggests that neurons may regulate dendritic and axonal connectivity, as well as intrinsic excitability in response to perturbations in order to stabilize function (Tien and Kerschensteiner, 2018; Turrigiano, 2012). Recent studies have also suggested that retinal remodeling is an adaptive process to maintain visual function, rather than being solely destructive. Homeostatic plasticity in the retina and visual cortex in RP helps maintain normal vision even when more than half of the rod photoreceptors are lost (Begenisic et al., 2020; Care et al., 2020). Rewiring cone-cone bipolar cells or potentiating rod-rod bipolar cell signaling preserves light responses in

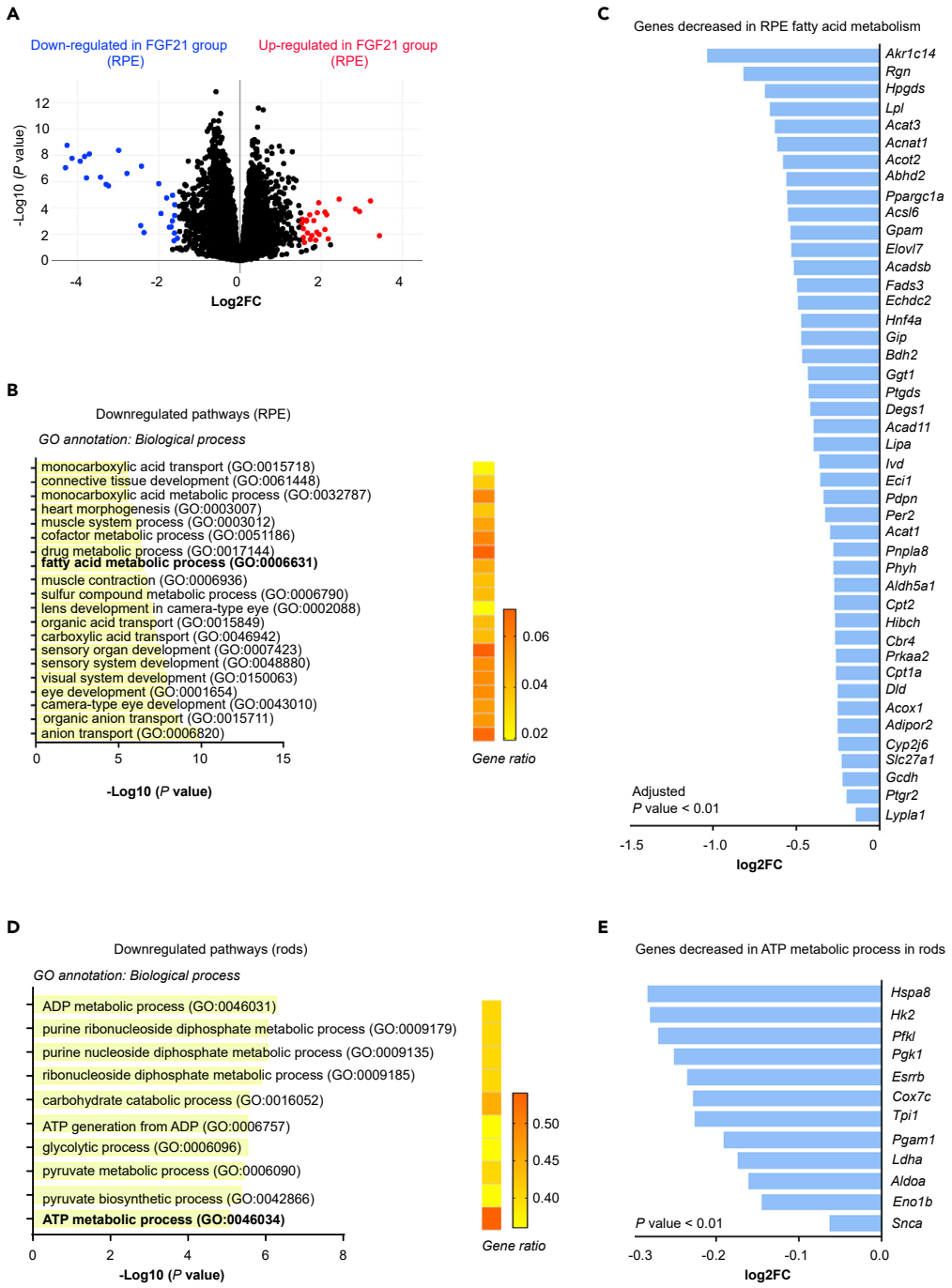

Figure 6. FGF21 decreased RPE and rod metabolism in P23H mice

(A) RPE cells were isolated and RNA was extracted for RNAseq. Littermate mice were used. n = 3 mice per group. Pathways were identified with gene ontology. p values for enriched gene ontology (GO) terms are showed in bar graphs ($P < 0.01$).

(B) Most downregulated genes in RPE cell population by FGF21 were associated with metabolism. p values for enriched gene ontology (GO) terms are showed in bar graphs ($P < 0.01$). Gene ratio for each pathway was shown in heatmap.

(C) Genes involved in fatty acid metabolic process (GO:0006631) were downregulated by FGF21 in RPE cells in P23H mice. Bar graph showing fold change (in log2) of indicated genes in FGF21 vs vehicle.

(D) Genes involved in ATP metabolic process (GO:0046034) were downregulated by FGF21 in rods in P23H mice.

(E) Bar graph showing fold change (in log2) of indicated genes in rod ATP metabolic process in FGF21 vs vehicle.

See also Figures S3 and S6.

photoreceptor-degenerating mice (Leinonen et al., 2020; Shen et al., 2020). Bipolar cells also participate in compensatory dendritic remodeling and synapse formation in response to the loss of photoreceptors (Beier et al., 2017, 2018; Care et al., 2019; Johnson et al., 2017; Shen et al., 2020). Therefore, modulating retinal remodeling in response to photoreceptor loss may help maintain or improve retinal function in response to retinal degeneration.

Our single-cell transcriptomics data showed that FGF21 upregulated pathways involved in axon development and synapse formation in retinal Müller glia/astrocytes (Figures 4A and 4B). This is consistent with results from cell culture in which postsynaptic currents in ganglion cells are enhanced by the presence of glia (Pfrieger and Barres, 1996, 1997). We also found that genes involved in synapse formation were also upregulated in amacrine cells (Figure S4). Taken together, these observations suggest that promoting neural and glial remodeling in P23H mouse retinas was associated with improved photoreceptor function.

Our gene set enrichment analysis showed that SRF motif was enriched in Müller glia in FGF21-treated P23H mice. SRF is crucial in axon guidance and circuit formation. SRF is a ubiquitous transcription factor that mediates brain-derived neurotrophic factor protection of postnatal cortical neurons against camptothecin or trophic deprivation (Chang et al., 2004). SRF is crucial in axon guidance and circuit formation in the hippocampus (Knoll et al., 2006). Deficiency of *Srf* in mice reduces neurite outgrowth and abolishes mossy fiber segregation (Knoll et al., 2006). In the adult brain, SRF deficiency impairs synaptic plasticity (Ramanan et al., 2005). Conditional prenatal *Srf* deletion also impairs neuronal migration of the rostral migratory stream (Alberti et al., 2005). Therefore, modulating retinal glia-specific SRF might regulate retinal remodeling (improved Müller glia structure with GLUL and GFAP staining) and potentially influence retinal neural function. However, we did not observe remarkable changes of synapse gene expression in rMC-1 cells treated with SRF siRNAs (~60% decrease in *Srf* mRNA levels, data not shown). We speculated that loss of cell-cell contact *in vitro* might diminish the synapse gene expression in glial cells.

The severity of visual field loss (and loss of retinal function) in patients with RP correlates with retinal vessel attenuation (Ma et al., 2012; Nakagawa et al., 2014). In RP animal models, progressive retinal vessel loss is specifically found in the OPL (adjacent to the photoreceptor nuclear layer) (Fernandez-Sanchez et al., 2018; Hanna et al., 2018). Müller glia might mediate the vascular response to photoreceptor loss as they are the primary source of neurotrophic/angiogenic factors such as vascular endothelial growth factors (Bai et al., 2009; Jiang et al., 2014; Pierce et al., 1995; Saint-Geniez et al., 2008; Wang et al., 2010). Single-cell transcriptomics showed that FGF21 versus vehicle treatment increased *Vegf* expression in Müller glia/astrocytes (LogFC = 0.1837, $P < 0.01$) in P23H mice, further suggesting the involvement of Müller glia in the impact of FGF21 on retinal remodeling in P23H mice.

In addition to Müller glial changes, in P23H mouse RPE cells, we found that FGF21 decreased expression of genes involved in fatty acid metabolism (Figures 6A–6C), metabolically corresponding to the decreased ATP metabolic processes we found in rod photoreceptors (Figures 6D and 6E). Less is known about cellular sources of lipid to photoreceptor energy metabolism, although RPE cells are tightly linked to photoreceptor metabolism (Fu et al., 2020). RPE cells produce and transfer fatty acids (such as palmitate, 11-cis-retinal, and ketone bodies) to photoreceptors to ensure proper visual function (Bibb and Young, 1974; Orban et al., 2011; Palczewski, 2010; Puchalska and Crawford, 2017). RPE cells preferentially pass glucose to photoreceptors, and photoreceptors then metabolize glucose to lactate, which is transferred back for RPE use as fuel (seen *in vitro)* (Kanow et al., 2017; Strauss, 2005). However, in RPE cells *in vivo,* lactate might not be the major source of tricarboxylic acid cycle intermediates, as minimal metabolism from lactate to pyruvate is evident (Wang et al., 2019b), although flux studies are required to firmly establish this fact. Alternatively, fatty acid oxidation following phagocytosis of lipid-rich photoreceptor outer segments could be an energy source (Adijanto et al., 2014; Izuta et al., 2018; Reyes-Reveles et al., 2017). Compared to RPE from wild-type pigs, the RPE cells from pigs with retinal degeneration (RP) no longer have access to high levels of fatty acids as phagocytosis of photoreceptor outer segments diminishes with loss of photoreceptors and fatty acid beta oxidation decreases (Wang et al., 2019b). As rod outer segment tips shorten in RP, glucose metabolism increases in the RPE and there is diminished glucose transport to photoreceptors causing photoreceptor starvation (Wang et al., 2019b). Experimental loss of glycolysis in rods accelerates rod photoreceptor loss in RP. Enhancing rod glycolysis delays the loss of rod function (Zhang et al., 2016).

Because FGF21 decreased RPE fatty acid metabolism in P23H mice at postnatal week 10, we speculate that the long-term protective impacts of FGF21 on RP might be different than shorter term effects, in line with our finding that the protection of FGF21 on the cone pathway was no longer observed at postnatal week 13 (Figure S2).

In summary, we showed that FGF21 can improve rod and cone function in the P23H model of RP associated with modified Müller cell function affecting axon and synapse formation, as well as more normal Müller cell structure. Targeting Müller glial remodeling might be a general therapeutic approach to improve retinal function in RP. Homeostatic plasticity is associated with maintaining retinal function during photoreceptor degeneration. Previous reports have shown that the formation of new functional synapses between rods and rod bipolar cells restores rod function (Care et al., 2019; Johnson et al., 2017; Shen et al., 2020; Wang et al., 2019a). Our current finding suggests that Müller glia cells can modify retinal homeostatic plasticity via axon development and synapse formation.

Limitations of the study

The mechanism behind FGF21 activating Müller glial responses needs to be further validated. Alterations of Müller glial cell characteristics and lack of cell-cell contact *in vitro* limited a few of our current experimental explorations.

Resource availability

Lead contact

L.E.H.S will take the responsibilities as requested by *iScience*.

Materials availability

Mice, cell line, antibodies, and other reagents used in this study were commercially available, and company and catalog numbers were provided in Supplemental Experimental Procedures. PF-05231023 was under MTA with *Pfizer* but also commercially available at GLPBIO, Catalog No.GC31495.

Data and code availability

Raw data of single-cell transcriptomics and bulk RNA-seq data were deposited at SRA and can be accessed with Database NIH bioproject PRJNA625994.

METHODS

All methods can be found in the accompanying transparent methods supplemental file.

SUPPLEMENTAL INFORMATION

Supplemental information can be found online at https://doi.org/10.1016/j.isci.2021.102376.

ACKNOWLEDGMENT

L.E.H.S. is supported by NIH R24EY024868, R01EY017017, R01EY01717-13S1, R01EY030904, BCH IDDRC (1U54HD090255), Mass Lions Eye Foundation 75007; A.H. is supported by the Swedish Research Council (DNR# #2020-01092), government grants under the ALF agreement ALFGBG-717971, and the Wallenberg Clinical Scholars; Z.F. is supported by Boston Children's Hospital Manton Center for Orphan Disease Research 96307, OFD/BTREC/CTREC Faculty Career Development Grant 97906, and Ophthalmology Foundation 85010, Little Giraffe Foundation 75449, and Mass Lions Eye Foundation 87820; J.D.A. is supported by R01EY028953; C.Q. is supported by Alzheimer's Association Research Fellowship AARF-19-617868; Y.T. is supported by the Manpei Suzuki Diabetes Foundation, Alcon Research Institute 77486, and Bert M. Glaser, MD Award 80131.

AUTHOR CONTRIBUTION

Concept and design, L.E.H.S, Z.F., and S.T.; formal analysis, Z.F., C.Q., G.C., S.T., and L.E.H.S.; investigation, Z.F.; writing-original draft, Z.F., C.Q., and G.C.; writing-review & editing, L.E.H.S., A.H., and S.T.; resources, S.T.; funding acquisition, L.E.H.S.; methodology, Z.F., C.Q., G.C., Y.T., S.H., B.C., Y.K., W.A., E.B., JS.J., and J.D.A.; supervision, L.E.H.S, S.T., and A.H.

DECLARATION OF INTERESTS

The authors declare that the research was conducted in the absence of any commercial or financial relationships that could be construed as a potential conflict of interest. S.T. is an employee of Merck Sharp & Dohme Corp., a subsidiary of Merck & Co., Kenilworth, NJ, USA, and a stockholder in Merck & Co., Kenilworth, NJ, USA.

Received: January 19, 2021
Revised: February 13, 2021
Accepted: March 25, 2021
Published: April 23, 2021

REFERENCES

Adijanto, J., Du, J., Moffat, C., Seifert, E.L., Hurle, J.B., and Philp, N.J. (2014). The retinal pigment epithelium utilizes fatty acids for ketogenesis. J. Biol. Chem. *289*, 20570–20582.

Ait-Ali, N., Fridlich, R., Millet-Puel, G., Clerin, E., Delalande, F., Jaillard, C., Blond, F., Perrocheau, L., Reichman, S., Byrne, L.C., et al. (2015). Rod-derived cone viability factor promotes cone survival by stimulating aerobic glycolysis. Cell *161*, 817–832.

Akula, J.D., Hansen, R.M., Tzekov, R., Favazza, T.L., Vyhovsky, T.C., Benador, I.Y., Mocko, J.A., McGee, D., Kubota, R., and Fulton, A.B. (2010). Visual cycle modulation in neurovascular retinopathy. Exp. Eye Res. *91*, 153–161.

Alberti, S., Krause, S.M., Kretz, O., Philippar, U., Lemberger, T., Casanova, E., Wiebel, F.F., Schwarz, H., Frotscher, M., Schutz, G., et al. (2005). Neuronal migration in the murine rostral migratory stream requires serum response factor. Proc. Natl. Acad. Sci. U S A *102*, 6148–6153.

Bai, Y., Ma, J.X., Guo, J., Wang, J., Zhu, M., Chen, Y., and Le, Y.Z. (2009). Muller cell-derived VEGF is a significant contributor to retinal neovascularization. J. Pathol. *219*, 446–454.

Ban, Y., and Rizzolo, L.J. (2000). Regulation of glucose transporters during development of the retinal pigment epithelium. Brain Research. Dev. Brain Res. *121*, 89–95.

Begenisic, T., Mazziotti, R., Sagona, G., Lupori, L., Sale, A., Galli, L., and Baroncelli, L. (2020). Preservation of visual cortex plasticity in retinitis pigmentosa. Neuroscience *424*, 205–210.

Beier, C., Hovhannisyan, A., Weiser, S., Kung, J., Lee, S., Lee, D.Y., Huie, P., Dalal, R., Palanker, D., and Sher, A. (2017). Deafferented adult rod bipolar cells create new synapses with photoreceptors to restore vision. J. Neurosci. *37*, 4635–4644.

Beier, C., Palanker, D., and Sher, A. (2018). Stereotyped synaptic connectivity is restored during circuit repair in the adult mammalian retina. Curr. Biol. *28*, 1818–1824 e1812.

Bibb, C., and Young, R.W. (1974). Renewal of fatty acids in the membranes of visual cell outer segments. J. Cell Biol. *61*, 327–343.

Bookout, A.L., de Groot, M.H., Owen, B.M., Lee, S., Gautron, L., Lawrence, H.L., Ding, X., Elmquist, J.K., Takahashi, J.S., Mangelsdorf, D.J., et al. (2013). FGF21 regulates metabolism and circadian behavior by acting on the nervous system. Nat. Med. *19*, 1147–1152.

Bringmann, A., and Wiedemann, P. (2012). Muller glial cells in retinal disease. Ophthalmologica. *227*, 1–19.

Care, R.A., Anastassov, I.A., Kastner, D.B., Kuo, Y.M., Della Santina, L., and Dunn, F.A. (2020). Mature retina compensates functionally for partial loss of rod photoreceptors. Cell Rep. *31*, 107730.

Care, R.A., Kastner, D.B., De la Huerta, I., Pan, S., Khoche, A., Della Santina, L., Gamlin, C., Santo Tomas, C., Ngo, J., Chen, A., et al. (2019). Partial cone loss triggers synapse-specific remodeling and spatial receptive field rearrangements in a mature retinal circuit. Cell Rep. *27*, 2171–2183 e2175.

Chai, J., Norng, M., Tarnawski, A.S., and Chow, J. (2007). A critical role of serum response factor in myofibroblast differentiation during experimental oesophageal ulcer healing in rats. Gut *56*, 621–630.

Chang, S.H., Poser, S., and Xia, Z. (2004). A novel role for serum response factor in neuronal survival. J. Neurosci. *24*, 2277–2285.

Chen, H., and Anderson, R.E. (1993). Metabolism in frog retinal pigment epithelium of docosahexaenoic and arachidonic acids derived from rod outer segment membranes. Exp. Eye Res. *57*, 369–377.

Chen, S., Chen, S.T., Sun, Y., Xu, Z., Wang, Y., Yao, S.Y., Yao, W.B., and Gao, X.D. (2019). Fibroblast growth factor 21 ameliorates neurodegeneration in rat and cellular models of Alzheimer's disease. Redox Biol. *22*, 101133.

Denlinger, B., Helft, Z., Telias, M., Lorach, H., Palanker, D., and Kramer, R.H. (2020). Local photoreceptor degeneration causes local pathophysiological remodeling of retinal neurons. JCI Insight *5*, e132114.

Eisenfeld, A.J., Bunt-Milam, A.H., and Sarthy, P.V. (1984). Muller cell expression of glial fibrillary acidic protein after genetic and experimental photoreceptor degeneration in the rat retina. Invest. Ophthalmol. Vis. Sci. *25*, 1321–1328.

Fernandez-Sanchez, L., Esquiva, G., Pinilla, I., Lax, P., and Cuenca, N. (2018). Retinal vascular degeneration in the transgenic P23H rat model of retinitis pigmentosa. Front. Neuroanat. *12*, 55.

Fu, Z., Kern, T.S., Hellstrom, A., and Smith, L. (2020). Fatty acid oxidation and photoreceptor metabolic needs. J. Lipid Res., jlr.TR120000618.

Fu, Z., Wang, Z., Liu, C.H., Gong, Y., Cakir, B., Liegl, R., Sun, Y., Meng, S.S., Burnim, S.B., Arellano, I., et al. (2018). Fibroblast growth factor 21 protects photoreceptor function in type 1 diabetic mice. Diabetes *67*, 974–985.

Hanna, J., Yucel, Y.H., Zhou, X., Mathieu, E., Paczka-Giorgi, L.A., and Gupta, N. (2018). Progressive loss of retinal blood vessels in a live model of retinitis pigmentosa. Can. J. Ophthalmol. *53*, 391–401.

Haverkamp, S., and Wassle, H. (2000). Immunocytochemical analysis of the mouse retina. J. Comp. Neurol. *424*, 1–23.

Hill, C.M., Laeger, T., Dehner, M., Albarado, D.C., Clarke, B., Wanders, D., Burke, S.J., Collier, J.J., Qualls-Creekmore, E., Solon-Biet, S.M., et al. (2019). FGF21 signals protein status to the brain and adaptively regulates food choice and metabolism. Cell Rep. *27*, 2934–2947 e2933.

Hultman, K., Scarlett, J.M., Baquero, A.F., Cornea, A., Zhang, Y., Salinas, C.B.G., Brown, J., Morton, G.J., Whalen, E.J., Grove, K.L., et al. (2019). The central fibroblast growth factor receptor/beta klotho system: comprehensive mapping in Mus musculus and comparisons to nonhuman primate and human samples using an automated in situ hybridization platform. J. Comp. Neurol. *527*, 2069–2085.

Izuta, Y., Imada, T., Hisamura, R., Oonishi, E., Nakamura, S., Inagaki, E., Ito, M., Soga, T., and Tsubota, K. (2018). Ketone body 3-hydroxybutyrate mimics calorie restriction via the Nrf2 activator, fumarate, in the retina. Aging Cell *17*, e12699.

Jablonski, M.M., and Iannaccone, A. (2000). Targeted disruption of Muller cell metabolism induces photoreceptor dysmorphogenesis. Glia *32*, 192–204.

Jiang, Y., Wang, H., Culp, D., Yang, Z., Fotheringham, L., Flannery, J., Hammond, S., Kafri, T., and Hartnett, M.E. (2014). Targeting Muller cell-derived VEGF164 to reduce intravitreal neovascularization in the rat model of retinopathy of prematurity. Invest. Ophthalmol. Vis. Sci. *55*, 824–831.

Johnson, R.E., Tien, N.W., Shen, N., Pearson, J.T., Soto, F., and Kerschensteiner, D. (2017).

Homeostatic plasticity shapes the visual system's first synapse. Nat. Commun. *8*, 1220.

Jones, B.W., and Marc, R.E. (2005). Retinal remodeling during retinal degeneration. Exp. Eye Res. *81*, 123–137.

Jones, B.W., Pfeiffer, R.L., Ferrell, W.D., Watt, C.B., Marmor, M., and Marc, R.E. (2016). Retinal remodeling in human retinitis pigmentosa. Exp. Eye Res. *150*, 149–165.

Jones, B.W., Watt, C.B., Frederick, J.M., Baehr, W., Chen, C.K., Levine, E.M., Milam, A.H., Lavail, M.M., and Marc, R.E. (2003). Retinal remodeling triggered by photoreceptor degenerations. J. Comp. Neurol. *464*, 1–16.

Kanow, M.A., Giarmarco, M.M., Jankowski, C.S., Tsantilas, K., Engel, A.L., Du, J., Linton, J.D., Farnsworth, C.C., Sloat, S.R., Rountree, A., et al. (2017). Biochemical adaptations of the retina and retinal pigment epithelium support a metabolic ecosystem in the vertebrate eye. Elife *6*, e28899.

Katsu-Jimenez, Y., and Gimenez-Cassina, A. (2019). Fibroblast growth Factor-21 promotes ketone body utilization in neurons through activation of AMP-dependent kinase. Mol. Cell. Neurosci. *101*, 103415.

Kevany, B.M., and Palczewski, K. (2010). Phagocytosis of retinal rod and cone photoreceptors. Physiology (Bethesda) *25*, 8–15.

Kiser, P.D., and Palczewski, K. (2010). Membrane-binding and enzymatic properties of RPE65. Prog. Retin. Eye Res. *29*, 428–442.

Knoll, B., Kretz, O., Fiedler, C., Alberti, S., Schutz, G., Frotscher, M., and Nordheim, A. (2006). Serum response factor controls neuronal circuit assembly in the hippocampus. Nat. Neurosci. *9*, 195–204.

Koulen, P., Fletcher, E.L., Craven, S.E., Bredt, D.S., and Wassle, H. (1998). Immunocytochemical localization of the postsynaptic density protein PSD-95 in the mammalian retina. J. Neurosci. *18*, 10136–10149.

Krishnamoorthy, V., Cherukuri, P., Poria, D., Goel, M., Dagar, S., and Dhingra, N.K. (2016). Retinal remodeling: concerns, emerging remedies and future prospects. Front. Cell. Neurosci. *10*, 38.

Leinonen, H., Pham, N.C., Boyd, T., Santoso, J., Palczewski, K., and Vinberg, F. (2020). Homeostatic plasticity in the retina is associated with maintenance of night vision during retinal degenerative disease. Elife *9*, e59422.

London, A., Benhar, I., and Schwartz, M. (2013). The retina as a window to the brain-from eye research to CNS disorders. Nat. Rev. Neurol. *9*, 44–53.

Ma, Y., Kawasaki, R., Dobson, L.P., Ruddle, J.B., Kearns, L.S., Wong, T.Y., and Mackey, D.A. (2012). Quantitative analysis of retinal vessel attenuation in eyes with retinitis pigmentosa. Invest. Ophthalmol. Vis. Sci. *53*, 4306–4314.

Mukherjee, P.K., Marcheselli, V.L., de Rivero Vaccari, J.C., Gordon, W.C., Jackson, F.E., and Bazan, N.G. (2007). Photoreceptor outer segment phagocytosis attenuates oxidative stress-induced apoptosis with concomitant neuroprotectin D1 synthesis. Proc. Natl. Acad. Sci. U S A *104*, 13158–13163.

Nagar, S., Krishnamoorthy, V., Cherukuri, P., Jain, V., and Dhingra, N.K. (2009). Early remodeling in an inducible animal model of retinal degeneration. Neuroscience *160*, 517–529.

Nakagawa, S., Oishi, A., Ogino, K., Makiyama, Y., Kurimoto, M., and Yoshimura, N. (2014). Association of retinal vessel attenuation with visual function in eyes with retinitis pigmentosa. Clin. Ophthalmol. *8*, 1487–1493.

Newman, E., and Reichenbach, A. (1996). The Muller cell: a functional element of the retina. Trends Neurosci. *19*, 307–312.

Newton, F., and Megaw, R. (2020). Mechanisms of photoreceptor death in retinitis pigmentosa. Genes (Basel) *11*, 1120.

O'Brien, E.E., Greferath, U., and Fletcher, E.L. (2014). The effect of photoreceptor degeneration on ganglion cell morphology. J. Comp. Neurol. *522*, 1155–1170.

Orban, T., Palczewska, G., and Palczewski, K. (2011). Retinyl ester storage particles (retinosomes) from the retinal pigmented epithelium resemble lipid droplets in other tissues. J. Biol. Chem. *286*, 17248–17258.

Palczewski, K. (2010). Retinoids for treatment of retinal diseases. Trends Pharmacol. Sci. *31*, 284–295.

Park, S.J., Kim, I.B., Choi, K.R., Moon, J.I., Oh, S.J., Chung, J.W., and Chun, M.H. (2001). Reorganization of horizontal cell processes in the developing FVB/N mouse retina. Cell Tissue Res. *306*, 341–346.

Park, S.J., Lim, E.J., Oh, S.J., Chung, J.W., Rickman, D.W., Moon, J.I., and Chun, M.H. (2004). Ectopic localization of putative AII amacrine cells in the outer plexiform layer of the developing FVB/N mouse retina. Cell Tissue Res. *315*, 407–412.

Pavan, B., and Dalpiaz, A. (2018). Retinal pigment epithelial cells as a therapeutic tool and target against retinopathies. Drug Discov. Today *23*, 1672–1679.

Peng, Y.W., Hao, Y., Petters, R.M., and Wong, F. (2000). Ectopic synaptogenesis in the mammalian retina caused by rod photoreceptor-specific mutations. Nat. Neurosci. *3*, 1121–1127.

Pfeiffer, R.L., Marc, R.E., Kondo, M., Terasaki, H., and Jones, B.W. (2016). Muller cell metabolic chaos during retinal degeneration. Exp. Eye Res. *150*, 62–70.

Pfrieger, F.W., and Barres, B.A. (1996). New views on synapse-glia interactions. Curr. Opin. Neurobiol. *6*, 615–621.

Pfrieger, F.W., and Barres, B.A. (1997). Synaptic efficacy enhanced by glial cells in vitro. Science *277*, 1684–1687.

Pierce, E.A., Avery, R.L., Foley, E.D., Aiello, L.P., and Smith, L.E. (1995). Vascular endothelial growth factor/vascular permeability factor expression in a mouse model of retinal neovascularization. Proc. Natl. Acad. Sci. U S A *92*, 905–909.

Pierce, E.A., and Bennett, J. (2015). The status of RPE65 gene therapy trials: safety and efficacy. Cold Spring Harb. Perspect. Med. *5*, a017285.

Puchalska, P., and Crawford, P.A. (2017). Multi-dimensional roles of ketone bodies in fuel metabolism, signaling, and therapeutics. Cell Metab. *25*, 262–284.

Punzo, C., Kornacker, K., and Cepko, C.L. (2009). Stimulation of the insulin/mTOR pathway delays cone death in a mouse model of retinitis pigmentosa. Nat. Neurosci. *12*, 44–52.

Ramanan, N., Shen, Y., Sarsfield, S., Lemberger, T., Schutz, G., Linden, D.J., and Ginty, D.D. (2005). SRF mediates activity-induced gene expression and synaptic plasticity but not neuronal viability. Nat. Neurosci. *8*, 759–767.

Reyes-Reveles, J., Dhingra, A., Alexander, D., Bragin, A., Philp, N.J., and Boesze-Battaglia, K. (2017). Phagocytosis-dependent ketogenesis in retinal pigment epithelium. J. Biol. Chem. *292*, 8038–8047.

Riepe, R.E., and Norenburg, M.D. (1977). Muller cell localisation of glutamine synthetase in rat retina. Nature *268*, 654–655.

Sa-Nguanmoo, P., Chattipakorn, N., and Chattipakorn, S.C. (2016a). Potential roles of fibroblast growth factor 21 in the brain. Metab. Brain Dis. *31*, 239–248.

Sa-Nguanmoo, P., Tanajak, P., Kerdphoo, S., Satjaritanun, P., Wang, X., Liang, G., Li, X., Jiang, C., Pratchayasakul, W., Chattipakorn, N., et al. (2016b). FGF21 improves cognition by restored synaptic plasticity, dendritic spine density, brain mitochondrial function and cell apoptosis in obese-insulin resistant male rats. Horm. Behav. *85*, 86–95.

Saint-Geniez, M., Maharaj, A.S., Walshe, T.E., Tucker, B.A., Sekiyama, E., Kurihara, T., Darland, D.C., Young, M.J., and D'Amore, P.A. (2008). Endogenous VEGF is required for visual function: evidence for a survival role on muller cells and photoreceptors. PLoS One *3*, e3554.

Sakami, S., Imanishi, Y., and Palczewski, K. (2019). Muller glia phagocytose dead photoreceptor cells in a mouse model of retinal degenerative disease. FASEB J. *33*, 3680–3692.

Sarthy, V.P., Brodjian, S.J., Dutt, K., Kennedy, B.N., French, R.P., and Crabb, J.W. (1998). Establishment and characterization of a retinal Muller cell line. Invest. Ophthalmol. Vis. Sci. *39*, 212–216.

Shen, N., Wang, B., Soto, F., and Kerschensteiner, D. (2020). Homeostatic plasticity shapes the retinal response to photoreceptor degeneration. Curr. Biol. *30*, 1916–1926 e1913.

Stogsdill, J.A., and Eroglu, C. (2017). The interplay between neurons and glia in synapse development and plasticity. Curr. Opin. Neurobiol. *42*, 1–8.

Strauss, O. (2005). The retinal pigment epithelium in visual function. Physiol. Rev. *85*, 845–881.

Tien, N.W., and Kerschensteiner, D. (2018). Homeostatic plasticity in neural development. Neural Dev. *13*, 9.

Turrigiano, G. (2012). Homeostatic synaptic plasticity: local and global mechanisms for stabilizing neuronal function. Cold Spring Harb. Perspect. Biol. *4*, a005736.

Vecino, E., Rodriguez, F.D., Ruzafa, N., Pereiro, X., and Sharma, S.C. (2016). Glia-neuron interactions in the mammalian retina. Prog. Retin. Eye Res. *51*, 1–40.

Wang, J., Xu, X., Elliott, M.H., Zhu, M., and Le, Y.Z. (2010). Muller cell-derived VEGF is essential for diabetes-induced retinal inflammation and vascular leakage. Diabetes *59*, 2297–2305.

Wang, Q., Yuan, J., Yu, Z., Lin, L., Jiang, Y., Cao, Z., Zhuang, P., Whalen, M.J., Song, B., Wang, X.J., et al. (2018). FGF21 attenuates high-fat diet-induced cognitive impairment via metabolic regulation and anti-inflammation of obese mice. Mol. Neurobiol. *55*, 4702–4717.

Wang, T., Pahlberg, J., Cafaro, J., Frederiksen, R., Cooper, A.J., Sampath, A.P., Field, G.D., and Chen, J. (2019a). Activation of rod input in a model of retinal degeneration reverses retinal remodeling and induces formation of functional synapses and recovery of visual signaling in the adult retina. J. Neurosci. *39*, 6798–6810.

Wang, W., Kini, A., Wang, Y., Liu, T., Chen, Y., Vukmanic, E., Emery, D., Liu, Y., Lu, X., Jin, L., et al. (2019b). Metabolic deregulation of the blood-outer retinal barrier in retinitis pigmentosa. Cell Rep. *28*, 1323–1334 e1324.

Wang, X., Iannaccone, A., and Jablonski, M.M. (2004). Contribution of Muller cells toward the regulation of photoreceptor outer segment assembly. Neuron Glia Biol. *1*, 291–296.

Yu, Y., Bai, F., Wang, W., Liu, Y., Yuan, Q., Qu, S., Zhang, T., Tian, G., Li, S., Li, D., et al. (2015). Fibroblast growth factor 21 protects mouse brain against D-galactose induced aging via suppression of oxidative stress response and advanced glycation end products formation. Pharmacol. Biochem. Behav. *133*, 122–131.

Zhang, L., Du, J., Justus, S., Hsu, C.W., Bonet-Ponce, L., Wu, W.H., Tsai, Y.T., Wu, W.P., Jia, Y., Duong, J.K., et al. (2016). Reprogramming metabolism by targeting sirtuin 6 attenuates retinal degeneration. J. Clin. Invest. *126*, 4659–4673.

iScience, Volume *24*

Supplemental information

Retinal glial remodeling by FGF21 preserves retinal function during photoreceptor degeneration

Zhongjie Fu, Chenxi Qiu, Gael Cagnone, Yohei Tomita, Shuo Huang, Bertan Cakir, Yumi Kotoda, William Allen, Edward Bull, James D. Akula, Jean-Sébastien Joyal, Ann Hellström, Saswata Talukdar, and Lois E.H. Smith

Supplemental Figures and Figure legends

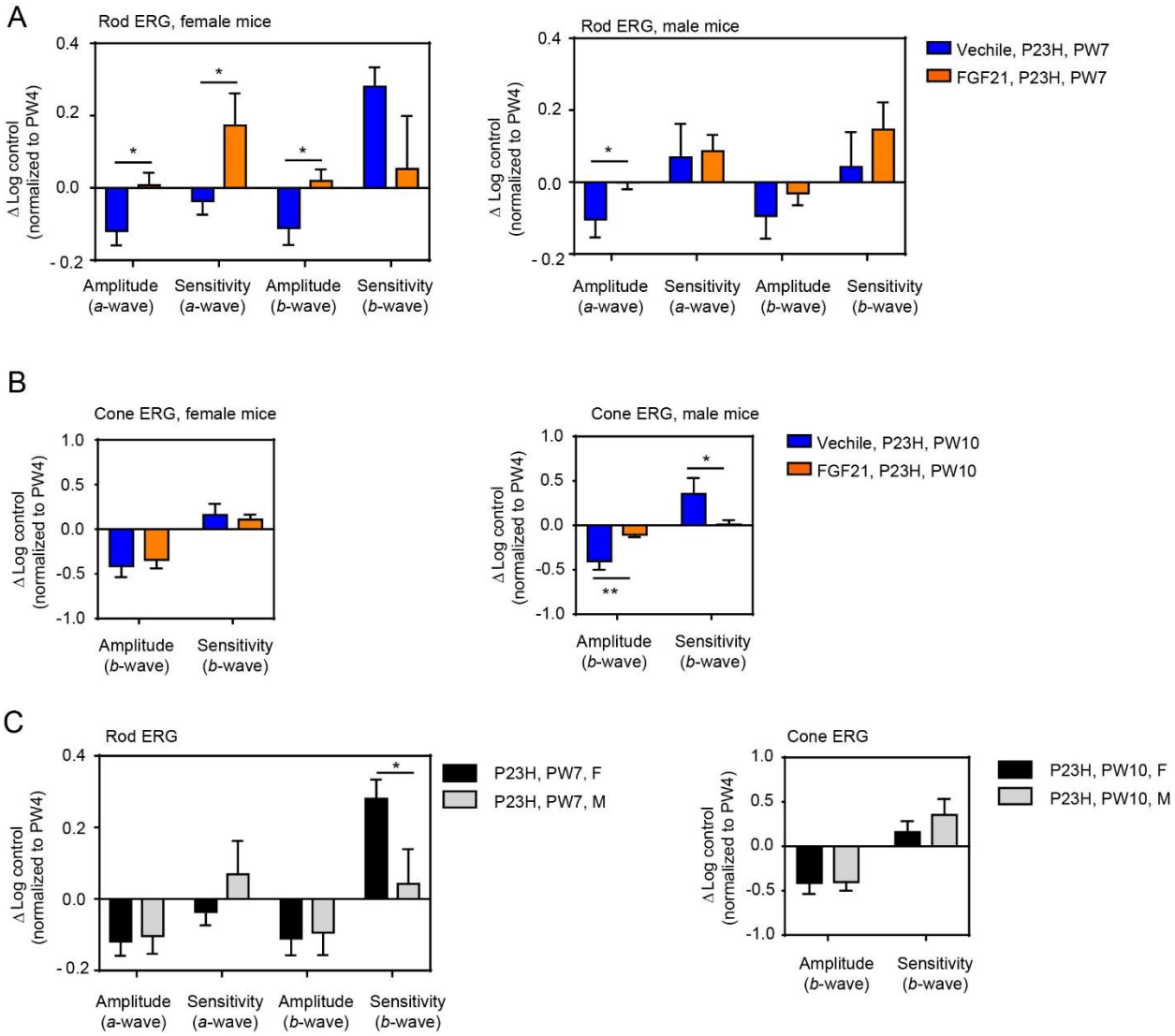

Supplemental Figure 1, related to Figure 1: Effects of FGF21 on ERG in female and male P23H mice respectively. Neuronal cell amplitude and sensitivity were measured and calculated. All ERG data were presented as the log change from control (ΔLog control) and normalized to that from postnatal week 4 (PW4). Data were presented as Mean±SEM.

A) FGF21 treatment attenuated the decrease in amplitude of rods and rod bipolar cell signals, as well as sensitivity of rod bipolar cells in female P23H mice at PW7 (vehicle, n=14-16 eyes; FGF21, n=11 eyes). FGF21 treatment attenuated the decrease in amplitude of rod signals in male P23H mice at PW7 (vehicle, n=14 eyes; FGF21, n=20 eyes). Multiple t-test. **P*<0.05.

B) FGF21 treatment attenuated the decrease in signal amplitude of bipolar cells and reduced induction in sensitivity of bipolar cells in male P23H mice at PW10 (vehicle, n=7-8 eyes, FGF21, n=10 eyes). No significant change was found in FGF21- vs vehicle-treated female P23H mice at PW10 (vehicle, n=6 eyes, FGF21, n=10 eyes). Multiple t-test. **P*<0.05, ***P*<0.01.

C) Female mice had a stronger induction of rod bipolar cell sensitivity in rod ERG at PW7 (n=14-16 eyes). No significant differences were found in cone ERG between male and female P23H mice (n=7-10 eyes). Multiple t-test. **P*<0.05.

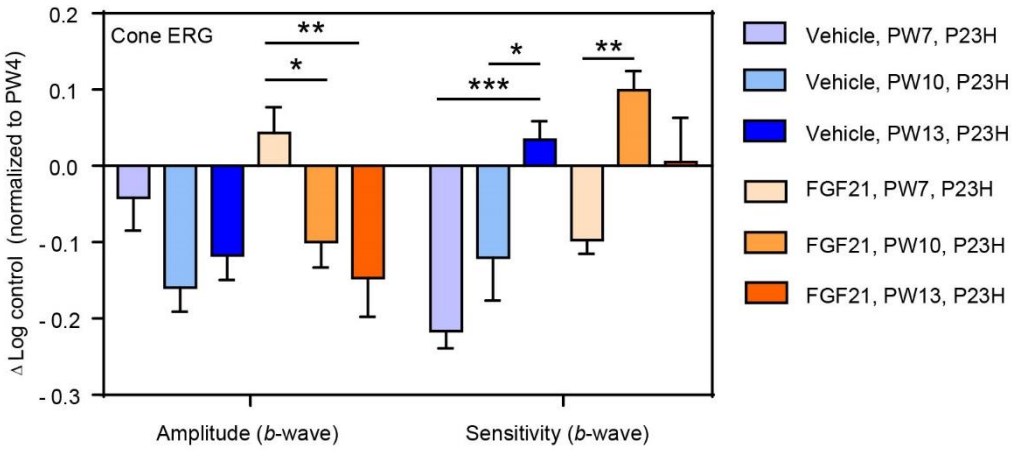

Supplemental Figure 2, related to Figure 1: Longitudinal impacts of FGF21 on cone pathway in P23H mice.

P23H mice were treated with FGF21 or vehicle from PW4. ERG was examined at PW7, PW10 and PW13 in the same mouse before and after treatment. All ERG data were presented as the log change from control (ΔLog control) and normalized to that from PW4. n=3-6 eyes per group. ANOVA. **P*<0.05, ***P*<0.01, ****P*<0.001. Data were presented as Mean±SEM.

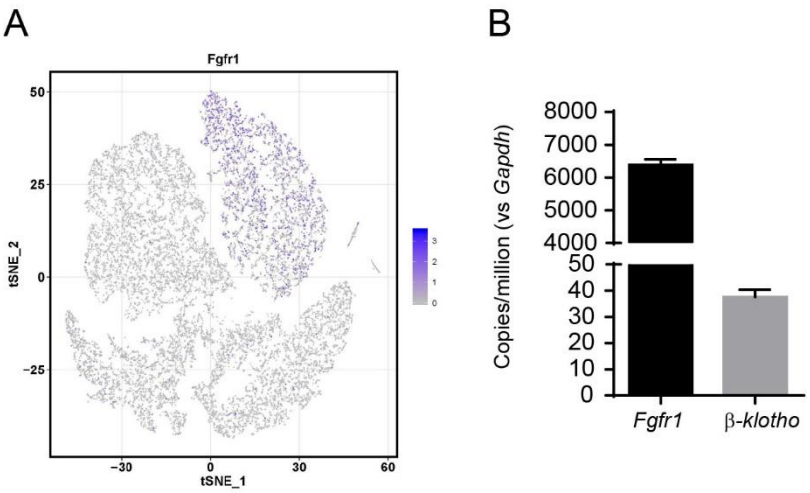

Supplemental Figure 3, related to Figure 3 & 6: Heat scatter map of *Fgfr1* in retinal clusters and expression of FGF21 receptors in RPE.
A) *Fgfr1* was mainly expressed in Müller glia/astrocyte cluster.
B) *Fgfr1* and β-*klotho* were expressed in mouse RPE with qPCR. *Gapdh* was used as internal reference. Data were presented as Mean±SEM.

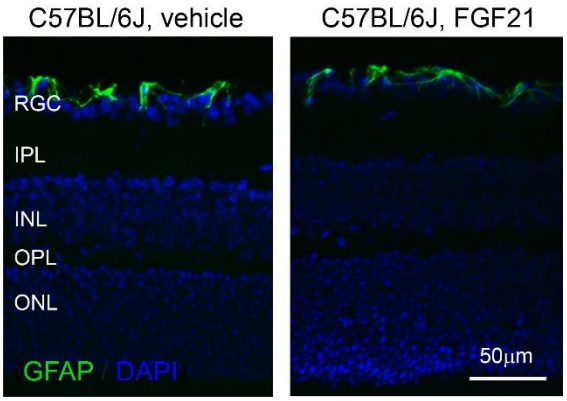

Supplemental Figure 4, related to Figure 4: Comparable GFAP signals in FGF21- vs. vehicle-treated C57BL/6J mice. C57BL/6J mice were treated with FGF21 or vehicle twice a week from PW4 to PW10. Retinal glial activation was examined with GFAP staining (green). DAPI (blue) was used for nuclear staining. Scale bar, 50μm.

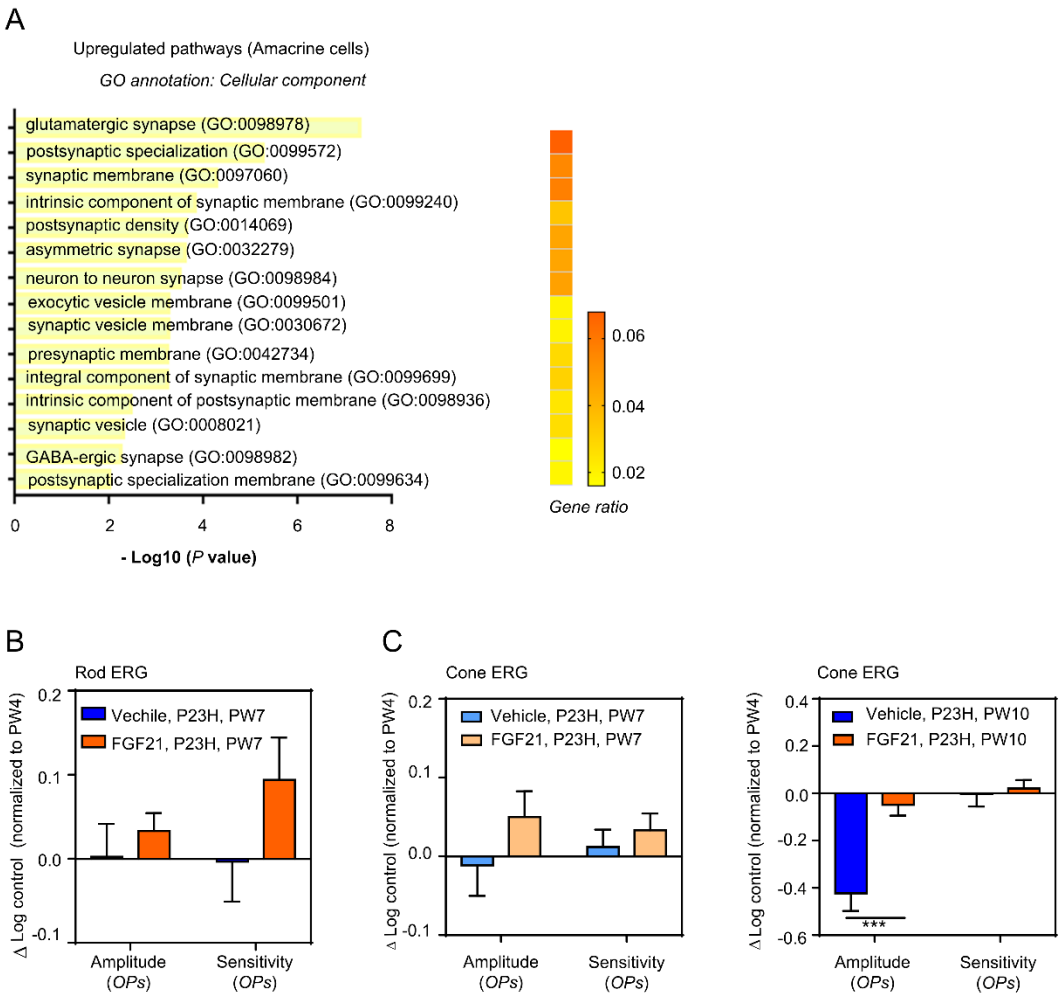

Supplemental Figure 5, related to Figure 4: FGF21 improved amacrine cell signaling in P23H mice.

A) Expression of genes involved in synapse formation was increased in amacrine cells in FGF21- vs. vehicle-treated P23H mouse retinas. The largest FGF21-induced increases in gene expression in amacrine cell population were associated with synapse formation. P-values for enriched gene-ontology (GO) terms are shown in bar graphs (P<0.01). Gene ratio for each pathway is shown in a heatmap.

B) Overall changes in rod OPs in P23H mice. FGF21 (PF-05231023)- versus control-treated group showed a trend of increased responses at PW7. All data were normalized to postnatal week 4. n=24-26 eyes. Multiple t-test. Data were presented as Mean±SEM.

C) Overall changes in cone OPs in P23H mice. FGF21 (PF-05231023)- versus control-treated mice showed comparable responses at PW7 but significantly increased OP amplitude at PW10. All data were normalized to postnatal week 4. n=17-30 eyes (vehicle), n=28-30 eyes (PF-05231023). Multiple t-test. ***P<0.001. Data were presented as Mean±SEM.

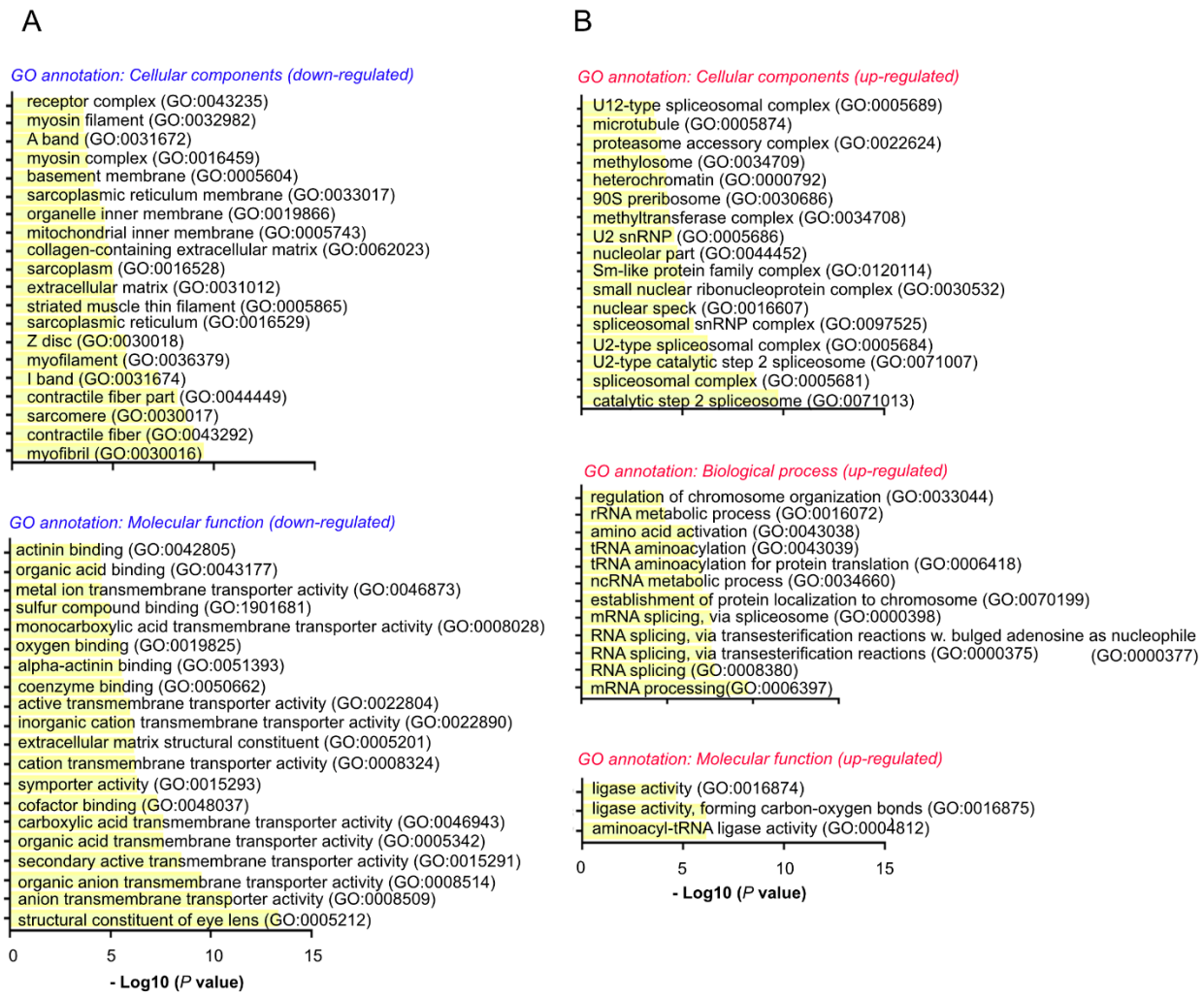

Supplemental Figure 6, related to Figure 6: FGF21 impact on RPE gene expression. RNAseq was conducted in isolated RPE cells from FGF21- vs vehicle-treated P23H littermates at PW10. Gene-ontology (GO) terms are showed in bar graphs (P<0.01).

Transparent Methods

Study Approval

All animal studies adhered to the Association for Research in Vision and Ophthalmology Statement for the Use of Animals in Ophthalmic and Vision Research and were approved by the Institutional Animal Care and Use Committee at Boston Children's Hospital (Protocol # 19-04-3913R).

FGF21 administration

The P23H refers to a proline to histidine substitution in codon 23 of rhodopsin (Dryja et al., 1990). This mutation has been found to contribute to RP. Of more than 100 rhodopsin mutations associated with RP (accounting for 30% of autosomal-dominant RP [adRP]) (Tam and Moritz, 2006), the P23H rhodopsin mutation is the most common (15-18% of adRP in the USA). The P23H mutation in mice causes decreased rod responses to light starting from postnatal week 5 with complete loss by postnatal week 25 (Sakami et al., 2011). Cone response loss starts from postnatal week 10 and there is a 90% reduction of cone signals by postnatal week 40 in heterozygous mice (Sakami et al., 2011). In our study, we examined retinal function using electroretinography (ERG), starting from postnatal week 4 when ERG is first feasible in these pups, with follow-up at postnatal weeks 7 and 10. We administered FGF21 following the initial ERG (postnatal week 4) and then throughout the course of study.

Homozygous P23H mice (B6.129S6(Cg)-*Rho*$^{tm1.1Kpal}$/J, Jackson Laboratory, #017628) were crossed with C57BL/6J mice (Jackson Laboratory, #000664) to generate heterozygous P23H mice. Unless otherwise indicated in this manuscript P23H refers to heterozygous P23H mice. The mouse tails were collected and genotyped at Transnetyx, Inc. Littermate heterozygous P23H mice were randomly assigned for treatment or vehicle groups. Postnatal-week-4 heterozygous P23H mice were intraperitoneally injected with 10 mg/kg long-acting FGF21 analog, PF-05231023 (*Pfizer*) (Huang et al., 2013) or vehicle (phosphate-buffered saline, PBS) control twice a week for six weeks. Retinal function was examined with ERG before treatment, 3 and 6 weeks after treatment. Both male and female mice were used. C57/BL6J mice were used to examine the impact of FGF21 on normal retinas. At postnatal week 10, mice were euthanized with overdose ketamine/xylazine and eyes were enucleated for sample collection.

Electroretinography (ERG)

ERG was used to assess the function of retinal neurons as we previously reported (Fu et al., 2017b; Fu et al., 2018). Flash ERGs were obtained using an Espion e^2 (Diagnosys LLC, Lowell, MA) in dark-adapted, mydriatic (Cyclomydril; Alcon, Fort Worth, TX), anesthetized (ketamine/xylazine) subjects. Stimuli were "green" light emitting diode flashes of doubling intensity from ~0.00025 to ~2.05 cd·s/m^2 and then "white" xenon-arc flashes from ~8.2 to ~1,050 cd·s/m^2 presented in an integrating sphere (Colordome, Diagnosys LLC). As shown (**Fig. 2A**), the saturating amplitude and sensitivity of the rod photoreceptors was estimated from the *a*-waves elicited by the white flashes (Lamb and Pugh, 1992). The saturating amplitude and sensitivity of second-order neurons, principally bipolar cells (Wurziger et al., 2001), was measured by subtracting this model from the intact ERG waveform (Robson and Frishman, 1995) and fitting the Naka-Rushton equation (Fulton and Rushton, 1978) to the response *vs*. intensity relationship of the resulting waveform, "P2". The oscillatory potentials (OPs), which characterize activity in inner retinal cells (amacrine cells and ganglion cells) distinct from the generators of the *a*- and *b*-waves (Dong et al., 2004), were filtered from P2 (Lei et al., 2006). For light-adapted ERG, stimuli were ~1.02 to 520 cd·s/m^2, the amplitude and sensitivity of cone bipolar cells was estimated from *b*-waves.

All ERG data were presented as the log change from control (ΔLogControl) at postnatal week 4; by expressing the data in log values, changes in observations of fixed proportion become linear, consistent with a constant fraction for physiologically meaningful changes in parameter values (Akula et al., 2008). Data from both eyes was included in all analyses. ΔLogControl ERG data were plotted as mean ± SEM.

Optical coherence tomography (OCT)

Mice were anesthetized (ketamine/xylazine) and mouse pupils were dilated with Cyclomydril (Alcon, Fort Worth, TX). Spectral domain OCT was performed with the image-guided OCT system (Micron IV, Phoenix Research Laboratories) (Fu et al., 2018). Photoreceptor thickness was measured using Insight software. The thickness of photoreceptors, including the outer nuclear layer and the inner/outer segment layer, was plotted at six distances (50, 100, 150, 200, 250 and 300 μm) from the optic nerve head, both on the nasal and on the temporal side (Fu et al., 2018).

Immunohistochemistry

For immunohistochemistry (IHC) on retinal cross-sections, eyes were fixed in 4% paraformaldehyde (PFA), frozen in optimal cutting temperature compound (OCT, Tissue-Tek) and then were cut into 10-μm sections. The sections were stored at -80^{o}C before use. The sections which included the optic nerve were treated with ice-cold methanol for 15 minutes, followed by 0.1% triton PBS for 30 minutes at room temperature, and then blocked with 3% bovine serum albumin (BSA) for 1 hour at room temperature. The sections were stained with primary antibody against glutamine synthetase (1:200, MAB302, Millipore), GFAP (1:500, ab4674, Abcam), PSD95 (1:250, 75-028, NeuroMab), cone arrestin (1:500, AB15282, Millipore), and rhodopsin (1:500, MABN15, Millipore) overnight at 4^{o}C. The sections were washed with PBS and then stained with a corresponding secondary antibody, covered in mounting medium with 4',6-Diamidine-2'-phenylindole dihydrochloride (DAPI, H-1200, Vector laboratories), and visualized with a Zeiss confocal microscope at 200X magnification.

Single-cell transcriptomics

Retinas from FGF21- vs vehicle-treated P23H littermates were carefully dissected with anterior segment and RPE cells removed. Single-cell suspensions were prepared from mouse retinas by using Worthington papain dissociation system. A retinal cell barcoded library was prepared at the Single Cell Core at Harvard Medical School (HMS) (Klein et al., 2015; Zilionis et al., 2017) and sequenced at Center for Cancer Computational Biology, Dana Farber Cancer Institute on a Nextseq500 with pair-end 75bp reads. Raw data were deposited at SRA and can be accessed with Database: NIH bioproject PRJNA625994.

scRNA-seq data is processed largely as previously described (Renthal et al., 2018), with slight modifications below. Reads were aligned to the mouse transcriptome GRCm38.81 by an inDrop pipeline to create a gene-cell counts matrix (Klein et al., 2015). Cells with less than 500 expressed genes (defined as read > 0) were filtered out. Cells with the fraction of mitochondrial genes six median absolute deviations higher than the median were further filtered out. An established pipeline was used to estimate the doublet score (Wolock et al., 2019), and cells with computed doublet score higher than 99% are considered putative doublets and filtered out. No significant batch effect was observed from principal component analysis.

Normalization and dimension reduction were performed using Seurat 3 following the manual (Butler et al., 2018). Briefly, expression for each cell was normalized, log transformed and globally scaled using NormalizeData, FindVariableFeatures and ScaleData functions from Seurat 3. PCA was also computed in Seurat 3, with number of principal components set to 100. FindNeighbors and FindClusters functions with default setting were used to determine the number of clusters, using the top 30 principal components. The top 30 principal components were subsequently subjected to tSNE clustering using RunTSNE function. For cell type identification, the expression profile of each cell was first compared to the existing profile from mouse cell atlas, and clusters with the vast majority of cells being the same cell type were analyzed further. Clusters of the same cell type were collapsed for further differential gene expression analyses, and the expression of known marker genes were cross-validated using VlnPlot and FeaturePlot functions.

For differential gene expression analyses, Genewise Negative Binomial Generalized Linear Models (glmFit model) of the edgeR package was employed (Robinson et al., 2010). The negative binomial distribution dispersion was estimated prior to modeling fitting using estimateDisp and glmFit functions. Log2 (fold change), p value and false discovery rate adjusted p value were computed for subsequent plotting (Yoav Benjamini, 1995). p value < 0.01 was taken as an arbitrary threshold for differentially expressed genes. In cases where indicated, an additional cutoff at false discovery rate adjusted p value was taken to further increase stringency. Differentially expressed genes were subjected to Gene-ontology analyses, as performed using clusterProfiler (Yu et al., 2012), and Gene set enrichment analysis (Subramanian et al., 2005).

Bulk RNAseq of RPE cells

After enucleation of mouse eyes from FGF21- vs vehicle-treated P23H littermates. The anterior segment and retina were removed and the remaining eye cup was immediately rinsed with PBS and transferred into 200µl RNAprotect cell reagent (Qiagen, #76526) (Xin-Zhao Wang et al., 2012). The eye cup was incubated for 15 minutes at room temperature and the tube was gently agitated to ensure most of the RPE cells were released. The eye cup was then removed before centrifuging the tubes at 2500rpm for 5 minutes at 4°C. The RPE cell pellets were then used for RNA extraction using a PureLink® RNA Mini Kit (#12183018A, Ambion).

Extracted RNA was quantified and good integrity samples (RIN>7) were processed for RNAseq analysis. Briefly, library preparation was done using the NEBNext Ultra II Directional mRNA kit, and sequencing was done on Illumina NextSeq 550 (75pb Single-Read). Fastq alignment and transcript count was performed using the kallisto pseudo aligner within the Biojupies platform (https://amp.pharm.mssm.edu/biojupies/). Volcano plot and biological annotation using enrichR were processed using Biojupies plug-ins as described in Torre et al, Cell Systems 2018 (Torre et al., 2018). Gene-ontology analyses were performed as described above. Raw data were deposited at SRA and can be accessed with Database: NIH bioproject PRJNA625994.

Real-time PCR

Retinas from P23H vs. WT littermates, FGF21- or vehicle-treated P23H littermates were lysed with QIAzol lysis reagent and incubated on ice for 15 minutes. 20% chloroform was added and incubated for 5 minutes at room temperature. RNA was extracted using a PureLink® RNA Mini Kit (#12183018A, Ambion) and then reverse transcribed using iScript™ cDNA synthesis kit (#1708891, Bio-Rad) (Fu et al., 2017a; Fu et al., 2018). qPCR was performed for glutamine synthetase (*Glul)*: 5'-TGA ACA AAG GCA TCA AGC AAA TG-3', 5'- CAG TCC AGG GTA CGG GTC TT-3'; *Fgfr1*: 5'-ACT CTG CGC TGG TTG AAA AAT-3', 5'-GGT GGC ATA GCG AAC CTT GTA-3'; *β-klotho*: 5'-TGT TCT GCT GCG AGC TGT TAC-3', 5'-CCG GAC TCA CGT ACT GTT TTT-3'. Quantitative analysis of gene expression was generated using an Applied Biosystems 7300 Sequence Detection System with the SYBR Green Master mix kit and gene expression was calculated relative to *Cyclophilin A* (5'-CAG ACG CCA CTG TCG CTT T-3'; 5'-TGT CTT TGG AAC TTT GTC TGC AA-3') or *Gapdh* (5'-GCC TAC ATG GCC TCC AAG G-3', 5'-GAG TTG GGA TAG GGC CTC TCT T-3') using the ΔΔCt method. Each sample was repeated in triplicate.

rMC-1 cell culture

Immortalized rat retinal Müller glial cells rMC-1 (Sarthy et al., 1998) (a gift from Dr. Jian-Xing Ma from University of Oklahoma) were cultured at 37°C, 5% CO_2 in a humidified atmosphere in DMEM/F12 medium (#11330057, Gibco) supplemented with 10% fetal bovine serum (#S12450, Atlanta Biologicals) and 1% antibiotic/antimycotic solution. An equal number of cells per well was plated on a 6-well dish. On the second day, the culture media were changed and the cells were treated with vehicle (PBS) or, 50, 500 ng/ml long-acting FGF21 (PF-05231023) for 24 hours. Cells were collected for protein.

Western blot

The levels of SRF were assessed in protein lysate from FGF21- vs vehicle-treated rMC-1 cells using (1:1000, Cell signaling, #5147s) in 5% non-fat milk (Labscientific, #M0841) overnight at 4°C. Signals were detected using 1:5000 corresponding horseradish peroxidase-conjugated secondary antibodies and enhanced chemiluminescence (ECL, Pierce), then the digital images were visualized with Bio-Rad ChemiDoc Touch Imaging System (Fu et al., 2018). β-ACTIN (1:5000, Sigma; A1978) was used as internal control.

Statistical analysis

Littermate male and female P23H mice were randomly assigned to FGF21 or vehicle treatments. The examiners were blinded to the treatment conditions during data analysis. The threshold for statistical significance (α) was set at 0.05. For the phenotypic study, sample size was computed by G*Power3 (Faul et al., 2007) to allow 80% power (set β to 0.2) with α set to 0.05. We collected the samples until reaching at least n=6 mice for each gender in treatment and vehicle groups. All data were presented as mean ± SEM. Two-tailed unpaired t-test, or ANOVA with Bonferroni's multiple comparison test was used for comparison of results as specified (Prism v5.0; GraphPad Software, Inc., San Diego, CA).

References

Akula, J.D., Mocko, J.A., Benador, I.Y., Hansen, R.M., Favazza, T.L., Vyhovsky, T.C., and Fulton, A.B. (2008). The neurovascular relation in oxygen-induced retinopathy. Molecular vision *14*, 2499-2508.

Butler, A., Hoffman, P., Smibert, P., Papalexi, E., and Satija, R. (2018). Integrating single-cell transcriptomic data across different conditions, technologies, and species. Nat Biotechnol *36*, 411-420.

Dryja, T.P., McGee, T.L., Reichel, E., Hahn, L.B., Cowley, G.S., Yandell, D.W., Sandberg, M.A., and Berson, E.L. (1990). A point mutation of the rhodopsin gene in one form of retinitis pigmentosa. Nature *343*, 364-366.

Faul, F., Erdfelder, E., Lang, A.G., and Buchner, A. (2007). G*Power 3: a flexible statistical power analysis program for the social, behavioral, and biomedical sciences. Behavior research methods *39*, 175-191.

Fu, Z., Gong, Y., Liegl, R., Wang, Z., Liu, C.H., Meng, S.S., Burnim, S.B., Saba, N.J., Fredrick, T.W., Morss, P.C., et al. (2017a). FGF21 Administration Suppresses Retinal and Choroidal Neovascularization in Mice. Cell reports *18*, 1606-1613.

Fu, Z., Lofqvist, C.A., Liegl, R., Wang, Z., Sun, Y., Gong, Y., Liu, C.H., Meng, S.S., Burnim, S.B., Arellano, I., et al. (2017b). Photoreceptor glucose metabolism determines normal retinal vascular growth. EMBO Mol Med.

Fu, Z., Wang, Z., Liu, C.H., Gong, Y., Cakir, B., Liegl, R., Sun, Y., Meng, S.S., Burnim, S.B., Arellano, I., et al. (2018). Fibroblast Growth Factor 21 Protects Photoreceptor Function in Type 1 Diabetic Mice. Diabetes *67*, 974-985.

Fulton, A.B., and Rushton, W.A. (1978). The human rod ERG: correlation with psychophysical responses in light and dark adaptation. Vision research *18*, 793-800.

Huang, J., Ishino, T., Chen, G., Rolzin, P., Osothprarop, T.F., Retting, K., Li, L., Jin, P., Matin, M.J., Huyghe, B., et al. (2013). Development of a novel long-acting antidiabetic FGF21 mimetic by targeted conjugation to a scaffold antibody. The Journal of pharmacology and experimental therapeutics *346*, 270-280.

Klein, A.M., Mazutis, L., Akartuna, I., Tallapragada, N., Veres, A., Li, V., Peshkin, L., Weitz, D.A., and Kirschner, M.W. (2015). Droplet barcoding for single-cell transcriptomics applied to embryonic stem cells. Cell *161*, 1187-1201.

Lamb, T.D., and Pugh, E.N., Jr. (1992). A quantitative account of the activation steps involved in phototransduction in amphibian photoreceptors. J Physiol *449*, 719-758.

Renthal, W., Boxer, L.D., Hrvatin, S., Li, E., Silberfeld, A., Nagy, M.A., Griffith, E.C., Vierbuchen, T., and Greenberg, M.E. (2018). Characterization of human mosaic Rett syndrome brain tissue by single-nucleus RNA sequencing. Nature neuroscience *21*, 1670-1679.

Robinson, M.D., McCarthy, D.J., and Smyth, G.K. (2010). edgeR: a Bioconductor package for differential expression analysis of digital gene expression data. Bioinformatics *26*, 139-140.

Robson, J.G., and Frishman, L.J. (1995). Response linearity and kinetics of the cat retina: the bipolar cell component of the dark-adapted electroretinogram. Vis Neurosci *12*, 837-850.

Sakami, S., Maeda, T., Bereta, G., Okano, K., Golczak, M., Sumaroka, A., Roman, A.J., Cideciyan, A.V., Jacobson, S.G., and Palczewski, K. (2011). Probing mechanisms of photoreceptor degeneration in a new mouse model of the common form of autosomal dominant retinitis pigmentosa due to P23H opsin mutations. The Journal of biological chemistry *286*, 10551-10567.

Sarthy, V.P., Brodjian, S.J., Dutt, K., Kennedy, B.N., French, R.P., and Crabb, J.W. (1998). Establishment and characterization of a retinal Muller cell line. Investigative ophthalmology & visual science *39*, 212-216.

Subramanian, A., Tamayo, P., Mootha, V.K., Mukherjee, S., Ebert, B.L., Gillette, M.A., Paulovich, A., Pomeroy, S.L., Golub, T.R., Lander, E.S., et al. (2005). Gene set enrichment

analysis: a knowledge-based approach for interpreting genome-wide expression profiles. Proceedings of the National Academy of Sciences of the United States of America *102*, 15545-15550.
Tam, B.M., and Moritz, O.L. (2006). Characterization of rhodopsin P23H-induced retinal degeneration in a Xenopus laevis model of retinitis pigmentosa. Investigative ophthalmology & visual science *47*, 3234-3241.
Torre, D., Lachmann, A., and Ma'ayan, A. (2018). BioJupies: Automated Generation of Interactive Notebooks for RNA-Seq Data Analysis in the Cloud. Cell Syst *7*, 556-561 e553.
Wolock, S.L., Lopez, R., and Klein, A.M. (2019). Scrublet: Computational Identification of Cell Doublets in Single-Cell Transcriptomic Data. Cell Syst *8*, 281-291 e289.
Wurziger, K., Lichtenberger, T., and Hanitzsch, R. (2001). On-bipolar cells and depolarising third-order neurons as the origin of the ERG-b-wave in the RCS rat. Vision Res *41*, 1091-1101.
Xin-Zhao Wang, C., Zhang, K., Aredo, B., Lu, H., and Ufret-Vincenty, R.L. (2012). Novel method for the rapid isolation of RPE cells specifically for RNA extraction and analysis. Experimental eye research *102*, 1-9.
Yoav Benjamini, Y.H. (1995). Controlling the False Discovery Rate: A Practical and Powerful Approach to Multiple Testing. Journal of the Royal Statistical Society. Series B (Methodological)

57, 289-300
Yu, G., Wang, L.G., Han, Y., and He, Q.Y. (2012). clusterProfiler: an R package for comparing biological themes among gene clusters. OMICS *16*, 284-287.
Zilionis, R., Nainys, J., Veres, A., Savova, V., Zemmour, D., Klein, A.M., and Mazutis, L. (2017). Single-cell barcoding and sequencing using droplet microfluidics. Nature protocols *12*, 44-73.